POLITECNICO DI TORINO

Master Degree in Communication and Computer Network Engineering

Master Degree Thesis

Phase Locked Loop for R-Mode navigation system

Author:
Filippo Giacomo RIZZI

Supervisor:
Prof. Fabio DOVIS

April 2020

A thesis submitted in fulfillment of the requirements for the Master degree in

Communications and Computer Networks Engineering

written in and financed by the

Nautical Systems department of the
Institute of Communication and Navigation of the
German Aerospace Center (DLR)

Abstract

Global Satellite Navigation Systems (GNSS) have become the primary Position, Navigation and Time (PNT) source in the maritime navigation domain, however natural and artificial interference may disrupt the GNSS signals causing performance degradation or service outages. In order to minimize the maritime navigational risk, a terrestrial backup system called Ranging Mode (R-Mode) is under development. Based on the signal of opportunity (SoOP) concept, the phase measurements of the medium frequency (MF) differential GNSS (DGNSS) signals can be exploited for positioning purposes. Among the possible techniques for phase estimation, the maximum likelihood (ML) and the discrete Fourier transform (DTFT) are currently used. Although they are suitable in a static scenario, for a dynamic one these techniques may be not the best choice since their performance are related to the observation time. In this work the phase locked loop (PLL) is considered as an alternative approach for phase estimation. The PLL design process is described and two self-interference mitigation techniques are proposed in order to improve its performance. The performance metrics are firstly assessed in a controlled simulated environment for validation, in both static and dynamic cases, and then applied on real measurement data.

Keywords: Signal Processing, Phase Locked Loop, Navigation Systems, Interference Mitigation

Acknowledgements

I would like to express my gratitude to the Nautical Systems Department of the DLR Institute of Communication and Navigation, particularly to Mr. Noack and Dr. Gewies for giving me the great opportunity to work for the DLR. Special thanks to my advisor Lars for his meticulous and friendly supervising activity during my stay in Neustrelitz. Words are not enough to express my gratitude to my supervisor Prof. Dovis for inspiring me with his precious lectures and his passion for the GNSS world. I express my gratitude to Prof. Carena for his useful laboratories and lectures that helped me for this work. My gratitude goes to Prof. Garello for his priceless lessons and for motivating me. Thanks to all my DLR colleagues, in particular to Daniel who always supported and encouraged me with his friendliness and to Frank for his outstanding competence and his incredibly tasty barbecues. My heartfelt thanks to my family, Mario, Linda, Angela, Pietro, Tonino and Angela for their immense love. My lovely thanks to Sonia for her daily support and lovely presence, helping me in the difficult moments. My gratitudes go to my friends Angelo, Giuseppe, Francesco and Angelo for letting me smile evryday with their funny stories. Thanks to Vincenzo, Caro, Yulia, Liang and Carlos for the nice time we spent together in the office and outside the working time. I am grateful to Ralf, Nico, Martin and all my volleyball teammates for the nice time we had playing together. Last but not least, I would like to thank my cousin Fabio for the limitless phone calls which supported and encouraged me during the writing time…

Contents

List of Figures

List of Tables

List of Abbreviations

ACCSEAS	**ACC**iessibility for **S**ipping, **E**fficiency **A**dvantages and **S**ustainability
AGC	**A**utomatic **G**ain **C**ontrol
AIS	**A**utomatic **I**dentification **S**ystem
AWGN	**A**dditive **W**hite **G**aussian **N**oise
CW	**C**ontinuous **W**ave
DGNSS	**D**ifferential **GNSS**
DLR	**D**eutsche Zentrum für **L**uft- und **R**aumfahrt
DTFT	**D**iscrete-**T**ime **D**ourier **T**ransform
GLONASS	**GLO**bal **Na**vigation **S**atellite **S**ystem
GNSS	**G**lobal **N**avigation **S**atellite **S**ystem
GPS	**G**lobal **P**ositioning **S**ystem
HDOP	**H**orizontal **D**ilution **O**f **P**recision
IALA	**I**nternational **A**ssociation of **L**ighthouse **A**uthorities
IMO	**I**nternational **M**aritime **O**rganization
LF	**L**oop **F**ilter
LORAN	**LO**ng **RA**nge **N**avigation
MF	**M**edium **F**requency
ML	**M**aximum **L**ikelihood
MSK	**M**inimum **S**hift **K**eying
NCO	**N**umerically **C**ontrolled **O**scillator
PDF	**P**robability **D**ensity **F**unction
PI	**P**roportional plus **I**ntegral
PLL	**P**hase **L**ocked **L**oop
PNT	**P**osition **N**avigation and **T**ime
PPS	**P**ulse **P**er **S**econd
RFI	**R**adio **F**requency **I**nterference
R-Mode	**R**anging **Mode**
SDPLL	**S**oftware **D**efined **P**hase **L**ocked **L**oop
SDR	**S**oftware **D**efined **R**adio
SoOP	**S**ignal **o**f **OP**portunity
TOA	**T**ime **O**f **A**rrival
TWSTT	**T**wo **W**ay **S**atellite **T**ime **T**ransfer
UTC	**U**niversal **C**oordinated **T**ime
VCO	**V**oltage **C**ontrolled **O**scillator
VDES	**V**HF **D**ata **E**xchange **S**ystem
VHF	**V**ery **H**igh **F**requency

Dedicated to my grandparents Maria and Mimino…

Chapter 1

Introduction

In the maritime domain, the art of navigation is well known in the history of humanity. The first sailors, equipped with sea charts, used reference points, such as celestial bodies to gather information about their own position on the earth. The positioning issue is strongly related to the time knowledge, indeed the lack of stable and accurate clock in the past was the critical braking point in order to obtain a good accuracy of latitude and longitude. A great advancement came with the No.4 marine chronometer developed by Jhon Harrison, which was tested in 1761 losing 5 seconds over an 81-day travel [1], improving largely the navigation capability. Nowadays, thanks to the huge technological enhancement, extremely stable and accurate clock are available, making possible the existence of positioning systems with millimeter-level accuracy [1].

In the last years many position and navigation systems were accessible for the maritime environment, based on different working principles, such as the Long RAnge Navigation (LORAN), the Omega, the Transit and the Chayka systems, but the advent of Global Navigation Satellite Systems (GNSS) has radically changed the situation becoming the principal trusted source replacing the other systems. The GNSS play a fundamental role not only in the maritime, but also in the aerospace, automotive and personal mobility domains as navigation systems. Their primary task is to provide position information to the user. Nevertheless, they are largely used in order to synchronize the electrical devices globally respect to a common reference time frame. As example it can be considered the synchronization of the power lines supply or the stock market. For these reasons, they are able to provide what is usually called Position, Navigation and Time (PNT) infrormation.

At the present, GNSS exist, the Global Positioning System (GPS) managed by United States of America, the European Galileo, the Russian GLObal NAvigation Satellite System (GLONASS) and the Chinese BeiDou, furthermore other regional satellite-based systems are usable, like the Japanese QZSS or the Indian NAVIC [2]. The great success of GNSS is mainly related to the global coverage, however the GNSS signals can be easily threatened by natural (ionospheric and tropospheric delays) and artificial interference due to their limited amount of power.

While the researchers are trying to study and model the effect of the natural interference in order to reduce its impact on GNSS signals,the number of intentional threats (jamming and or spoofing events) is dramatically increasing. In the maritime field, many events of interference have been reported. For example, the US Maritime Administration issued in November 2018 an advisory for GPS disruption in the Mediterranean Sea due to the armed conflict in Syria and suspected illegal fishing activities [3]. A further example can be found in [4], where a maritime measurement campaign, conducted by Deutsche Zentrum für Luft- und Raumfahrt (DLR), with the scope of identifying radio frequency interference (RFI) of GNSS signals onboard of a vessel is described and reported. Despite the positioning, many system interfaces on board of the vessels rely on GNSS compromising, in case of outage, the skipper to be able to navigate safely in a traditional manner [5].

In the literature, several ways have been taken into account to counteract to this type of events (e.g advanced signal processing techniques, adaptive antenna arrays and multi sensor fusion approaches [5]), and one of the possible solution is to rely on backup systems. A backup system is an independent system able to provide a reliable PNT solution and for the maritime domain the so called Ranging Mode (R-Mode) is under development [6].

1.1 Objective

The thesis was developed during a 9 month working experience at the Institute of Communication and Navigation of the DLR within the Nautical Systems department located in Neustrelitz (Germany), which is one of the twelve partners involved in the study and development of the R-Mode system. The R-Mode is based on the concept of reusing signals of existing maritime radio infrastructure for positioning purposes and in particular the phase of these signals can be exploited to determine the time of arrival (TOA) positioning. The focus of this study is on the Medium Frequency Differential GNSS (MF DGNSS) R-Mode signal, one of the possible existing signal which can be used in the R-Mode system and will be derived later on. At the time of writing, mamximum likelihood (ML) and discrete-time Fourier transform (DTFT) techniques were considered for the signal phase estimation. Although these techniques provide good accuracy and they are suitable for static applications, they have the main drawback of giving averaged information due to the observation time. The delay depends on the observation time and it can affect the position accuracy in a dynamic scenario, during the movement of vessels. In order to improve the receiver performance, an alternative approach can be given by the phase locked loop (PLL) architecture which is a control system able to estimate the phase of signals in real-time and sample by sample and it is inherently capable of adapting the phase estimate to signal dynamic variations due to ships movement. Therefore, this work is aimed to show the applicability and advantages of the PLL applied on the MF DGNSS R-Mode signal.

The work is organized as follows. Chapter 1 presents the R-Mode concept and some details about the challenging aspects of the system implementation. Moreover the MF DGNSS R-Mode is described and its signal presented. Chapter 2 introduces the theoretical information related to the phase estimation techniques. The ML and DTFT are presented but the chapter particularly focuses on the PLL working principles. Chapter 3 illustrates the design process and the challenging parameters setting of the PLL. Chapter 4 proposes two self-interference mitigation approaches needed to improve the PLL performance. The interference is caused by the signal structure and will be explained in this chapter. Chapter 5 shows the performance results of PLL phase estimation. The first part is devoted to simulated scenario in order to validate the proposed processing techniques whereas the second part presents the results obtained with real measurement. Last but not least, Chapter 6 presents the conclusion.

1.2 R-Mode

The R-Mode is meant to be a backup system for GNSS, by providing a reliable PNT service, improving the maritime navigation and increasing its safety. The R-Mode Baltic project is done in support of the EU INTERREG IVb North Sea Region Programme project ACCSEAS (Accessibility for Shipping, Efficiency Advantages and Sustainability) supporting the maritime access to the North Sea Region minimising navigational risk[7]. The system is based on the concept of Signal of OPportunity (SoOP), which means that existing infrastructures and signals can be reused for positioning purposes even though they are not designed for this duty. Consequently, some modifications and adjustments to the framework and signals could be needed to allow this task. Two main candidate signals are considered to be used, the Automaitc Identification System (AIS) and the MF DGNSS . Moreover, there is the possibility to combine the aforementioned systems with the LORAN-C/eLoran system in order to increase the number of signals to be used [7]. The investigation on further possibilities is an ongoing work at the time of writing and in the future there could be some other signals (such us the VHF Data Exchange System (VDES) which is the planned successor of the AIS [8]. This thesis focuses on the MF DGNSS, and all the work done is related to its signal that is described in the subsection 1.4.

The R-Mode Baltic project proposes a test bed located in the Baltic Sea in which 12 partners of maritime administrations, research institutions and private companies of Germany, Sweden, Norway and Poland are involved [9]. The test bed will use use modified marine radio beacons and AIS base stations to transmit R-Mode signals, with the objective to demonstrate that the R-Mode system is feasible and can be adopted worldwide [9].

1.3 R-Mode MF DGNSS

This work focuses on the R-Mode MF DGNSS marine radio beacons. The stations are actually used for Differential GNSS (DGNSS) and operate in the 283.5-325 kHz MF band. The signal contains correction and integrity information for GNSS receiver modulated as minimum shift keying (MSK), which is a continuous phase and constant amplitude modulation scheme, with a data rate of 100 or 200 bps. The system adopts a frequency reuse technique, as shown in Figure 1.1, among the transmitters to allocate channels and the spatial separation is used to reduce co-channel interference. There are different challenging issues to be solved, between them the time synchronization and the Sky wave reflection are the critical ones, but also the ground conductivity needs to be considered and accounted for having good performance [10]. It is important to point out that minimum performance requirement, need to be fulfilled for a safe navigation by considering the IMO guidelines [11], is to have an accuracy of at least 10 m with a probability of 95 %, for harbour entrances, harbour approaches and coastal waters navigation. Whereas for ocean waters navigation the accuracy rises up to 100 m with the same level of probability.

The synchronization of the stations to Universal Coordinated Time (UTC) can be obtained through [10]:

1. Two-way Satellite Time Transfer (TWSTT), requiring point-to-point links between transmitters and satellite;
2. eLORAN time receiver;
3. GPS time synchronization, until the signal is lost;
4. Self synchronization.

It is important to observe that for reaching good accuracy performance ($\leq$ 10 m) the stations need to be synchronized within 10 ns which is equivalent to 3 m in the space domain. Furthermore, the stability of the transmitters clock needs to be better than 1 ns, feasible for a Rubidium (10^{-11}) or Cesium clock (10^{-13}) [7].

The sky wave problem instead is a multipath effect generated by the signal reflection at the ionosphere. In a simple way, by considering just one reflected ray, it can be approximated as:

$$r(t) = s(t) + \alpha s(t - t_d) \tag{1.1}$$

where α and t_d respectively represent the attenuation factor and the delay of the sky wave. Depending on the reflecting path and the time delay, the ray can be seen as a constructive or destructive interference. The effect of this reflection is more sever far away from the transmitter because the ground wave can be more attenuated then the sky wave. In addition, the impact during the night is more relevant due to height changes of the ionosphere [10].

Also the geometrical displacement of the transmitters plays a fundamental role, in fact it directly affects the position accuracy. Of particular importance is the so called HDOP (Horizontal Dilution Of Precision) which is a value representing the impact of the transmitters location on the horizontal plane accuracy. Nevertheless, the HDOP is, in most of the North Sea area, less than 2 which is an acceptable value.

Figure 1.2 taken from [10] depicts the predicted accuracy in meters, based on TOA, in the North Sea area during the day (left) and night (right). The huge difference among them is mainly due to the sky wave effect. It is clear that for daytime most of the area is supported with an accuracy which is better than 10 m, fulfilling the requirements, while for the night time the performance can severely decrease compromising the system accuracy.

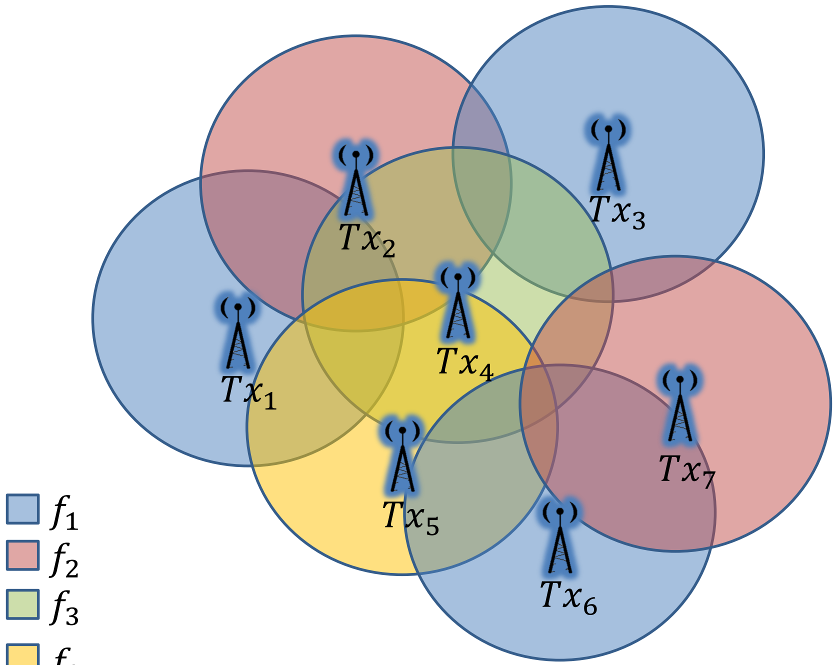

FIGURE 1.1: Frequency reuse concept: the transmitters 1, 3 and 6 uses frequency $f1$, the transmitters 2 and 7 uses frequency f2 while the transmitters 4 and 5 uses frequencies 3 and 4 without interfering

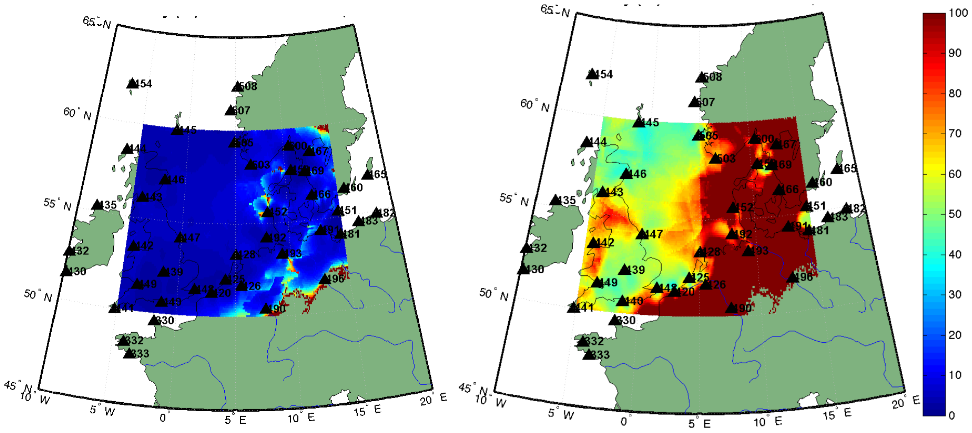

FIGURE 1.2: MF DGNSS R-Mode accuracy prediction in [m] for daytime (left) and night time (right) provided by [10]

1.4 MF DGNSS R-Mode Signal

The MF DGNSS signal is composed by an MSK (minumum shift keying) transmitting GNSS correction information with a bitrate R_b of 100 bps in Europe, while in some other regions a bitrate of 200 bps is used. The MSK maps each bit to a constant amplitude sinusoidal signal for T_b seconds, where $T_b = 1/R_b$. Two different frequencies are used. The MSK signal can be represented as [10]

$$s_{MSK}(t) = A \sin\left[2\pi\left(fc \pm b_k f\right)\left(t - kT_b\right) + \phi_k\right] \tag{1.2}$$

where A is the amplitude, f_c is the carrier frequency, $b_k = \pm 1$ depends on the transmitted data bit at time k, $f = R_b/4$ is the frequency change, while ϕ_k is the memory of the MSK which makes the phase of the signal continuous.

For ranging application the bit transitions or the phase of the MSK could be potentially exploited to estimate the TOA. The bit transition has an ambiguity of T_b seconds that, for the 100 bps message, means roughly 3000 km. Since the service range is expected to be in the order of 300 km, the bit time is unambiguous. Differently, the MSK phase is ambiguous because in the 300 kHz band the wavelength ,and consequently the lane width, is roughly 1 km. Due to the memory of the MSK the uncertainty is 250 m so that the ambiguity must be solved to extract the ranges [10]. The ambiguity issue is explained in

Section 2.1.

Although in theory the MSK phase can be used directly for ranging, a real practical implementation is challenging for different reasons such as the unknown sequence of transmitted data. Consequently, several possible solutions were taken into account in [10], and among them, the idea to add two continuous waves in the zero crossing of the MSK spectrum (to reduce disturbances of legacy receivers) was considered as the best option. Further modifications to the transmitted message could be considered in the future to improve performance of the system, but this is still under discussion and study. The resultant MF DGNSS R-Mode signal ($s_{RM}(t)$) can be written as the sum of three components

$$s_{RM}(t) = s_{MSK}(t) + s_{cw1}(t) + s_{cw2}(t) \tag{1.3}$$

where s_{MSK} is given in (1.2), while s_{cw1} and s_{cw2} are given as

$$\begin{cases} s_{cw_1}(t) = A_{cw_1} \sin(2\pi f_{cw_1} t + \phi_{cw_1}) \\ s_{cw_2}(t) = A_{cw_2} \sin(2\pi f_{cw_2} t + \phi_{cw_2}) \end{cases} \tag{1.4}$$

with

$$\begin{aligned} f_{cw_1} &= f_c - 225\ Hz \\ f_{cw_2} &= f_c + 225\ Hz \end{aligned} \tag{1.5}$$

and A_{cw_i}, ϕ_{cw_i} amplitude and phase offset for the i-th continuous wave.

In this work, it is assumed that the R-Mode signal is presented by (1.3) in Figure 1.3. A simulated power spectrum of the MF R-Mode signal is depicted. The central frequency of the station is assumed to be 303.5kHz and the three components (two continuous waves plus MSK) are pictured with different colors to highlight them.

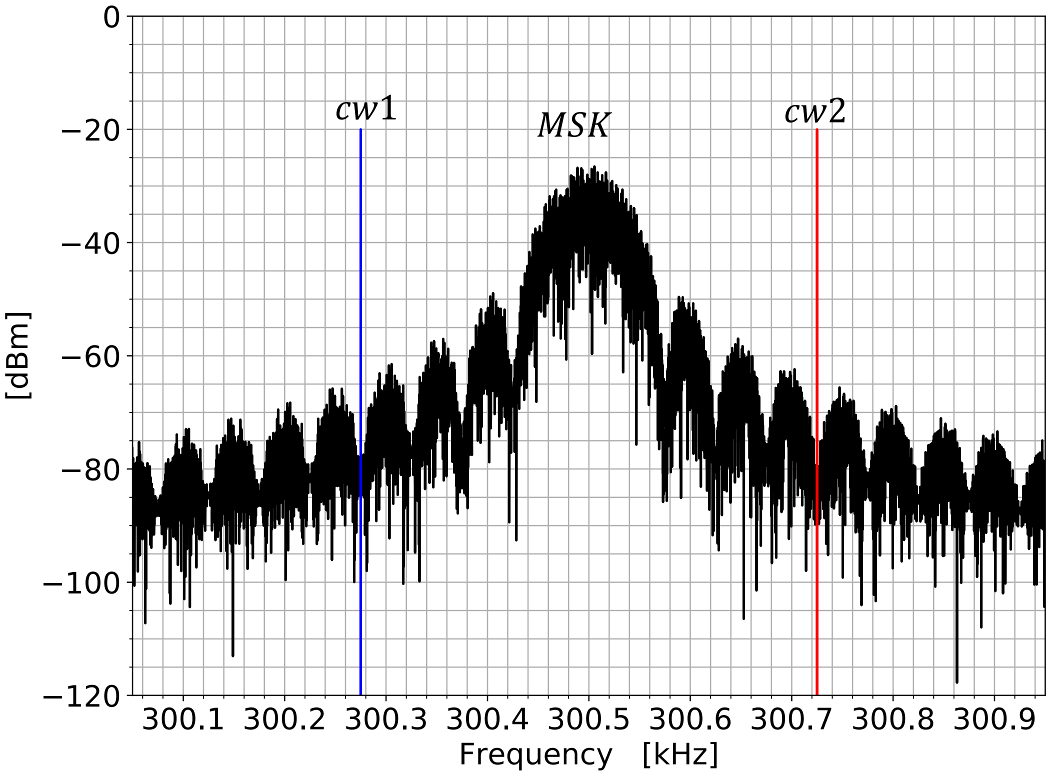

FIGURE 1.3: Power spectrum of a simulated MF DGNSS R-Mode signal without noise

Chapter 2

Phase Estimation and PLL Principles

This chapter is dedicated to the theoretical background needed to understand and develop the framework that supports the simulations and the results presented in Chapter 5.

2.1 Phase Ranging Technique

The phase of a signal holds the time information. It can be used for ranging applications. We can start by considering a continuous wave (CW) given as

$$CW(t) = b\sin(2\pi f t + \theta_0) \tag{2.1}$$

where f is the frequency of the CW and θ_0 is the initial phase at time t_0, while b is its constant amplitude. The link between the frequency of the signal and the wavelength is described as follows

$$\lambda = \frac{c}{f} \tag{2.2}$$

where λ is the wavelength of the signal with frequency f and c is the speed of light. The CW is characterized by cycles and each cycle (phase from 0 to 2π) corresponds to a distance equal to one wavelength.

An example is depicted in Figure 2.1, where the transmitter (Tx) sends two continuous waves at frequency $f_1 = 800$ and $f_2 = 3000$ Hz. Supposing that the initial phase, for both $\mathrm{CW_s}$ is zero, the receiver (Rx), which is located at 270 km from the transmitter, will measure a phase different from 0 and between $[0, 2\pi)$ due to the propagation path. For the two frequencies we get phases $\theta_1 = 4.52$ *rad* and $\theta_2 = 3.84$ *rad*. These phase values are transformed into distance measures by applying the following formula

$$r = \frac{\theta}{2\pi f}c = \frac{\theta}{2\pi}\lambda \tag{2.3}$$

and this results into two ranges $r_1 = 270$ km and $r_2 = 70$ km respectively for f_1 and f_2. The first frequency gives a correct result whereas the second one is affected by **ambiguity**. In the picture it can be seen that the signal at frequency f_2 performs two integer cycles before arriving at the receiver therefore we say that this measure is **ambiguous**, while the signal at frequency f_1 does not perform integer cycles hence we say this measure of the phase is **not ambiguous**. We can call ambiguity the number of integer cycles between the transmitter and the receiver and it is clear, by looking at the example, that depending on the frequency the receiver has to solve the ambiguity in order to obtain the true range.

As stated in Equation (2.2), the wavelength represents the distance in which the signal completes one cycle and for this particular example we have $\lambda_1 = 375$ and $\lambda_2 = 100$ km. By adding 2 wavelengths to r_2 we came up with correct range estimation. Summarizing, it can be said that, when the wavelength (linked to the frequency) is longer than the distance between the transmitter and the receiver the phase measurement will not be affected by the ambiguity, otherwise this problem must be addressed and solved. However this is possible only if the phase at the Tx side is known and in the case of the MF R-Mode signal it is known that at full second the phase of the CW at the transmitters must be zero hence the distance is obtained by looking at the delayed zero phase value. Concluding, Equation (2.3) is fundamental for our purposes and it is the formula used to obtain distances in the results presented in Chapter 5.

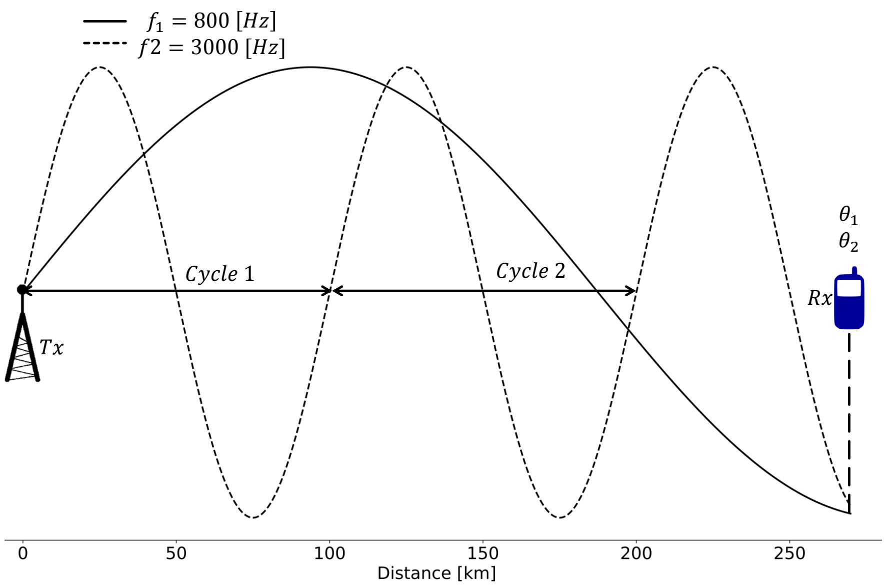

FIGURE 2.1: Example of phase ranging for two different frequencies

2.2 Phase Estimation Theory

The concept of phase ranging technique is introduced in Section 2.1 which shows how it is possible to obtain ranges by using phase measurements. Therefore, this section is dedicated to the phase estimation techniques.

These techniques are largely used in communication systems, mostly for synchronization purposes.

At the time of writing, the maximum likelihood (ML) estimation and the discrete time Fourier transform (DTFT) were used in order to estimate the phase of the R-Mode signal, thus a short introduction of these two methods is given in Section 2.2.1. A third approach, called PLL, is described in Section 2.2.2 and it constitutes the core part of this thesis.

2.2.1 Parametric Estimation

At the receiver side the signal is delayed and corrupted by noise, typically assumed to be additive white Gaussian noise (AWGN). The ML estimation allows us to obtain the parameters of the signal by maximizing the joint probability density function (PDF) of the received signal. In [12], a full derivation of the ML technique is presented and a detailed algorithm to implement such method is described. Here, a summary of the algorithm is presented by keeping the notation provided by [12].

First of all we consider the real signal as a single-tone

$$s(t) = b_0 \cos(\omega_0 t + \theta_0) \tag{2.4}$$

and the imaginary part (which can be obtained with the Hilbert transform)

$$\check{s}(t) = b_0 \sin(\omega_0 t + \theta_0) \tag{2.5}$$

The ML gives the estimate of b_0 and θ_0 for a given w_0 by using a noisy observation of the signal. We take a sampled version of the signal corrupted by AWGN noise $W(t)$ and a sampling time T such that

$$t_n = t_0 + nT \tag{2.6}$$

with $0 \leq n \leq N-1$ where N is the number of samples. The discrete-time complex signal is

$$\mathbf{Z} = \mathbf{X} + j\mathbf{Y} \tag{2.7}$$

where $\mathbf{X} = [X_0, X_1, ..., X_{N-1}]^T$ and $\mathbf{Y} = [Y_0, Y_1, ..., Y_{N-1}]^T$ with

$$X_n = s(t_n) + W(t_n) \qquad \text{for} \quad 0 \leq n \leq N-1 \tag{2.8}$$

$$Y_n = \check{s}(t_n) + \check{W}(t_n) \qquad \text{for} \quad 0 \leq n \leq N-1 \tag{2.9}$$

It is important to underline the fact that $\mathbf{Y}$ is the so called Hilbert Transform. The joint probability density function of the elements of $\mathbf{Z}$ when the parameters are unknown is given by

$$f(\mathbf{Z};\mathbf{a}) = \left(\frac{1}{\sigma^2 2\pi}\right)^N \exp\left[-\frac{1}{2\sigma^2}\sum_{n=0}^{N-1}(\mathbf{X}_n-\mu_n)^2+(\mathbf{Y}_n-\nu_n)^2\right] \tag{2.10}$$

where

$$\mathbf{a} = [\omega, b, \theta]^T \tag{2.11}$$

$$\mu_n = b_0\cos(\omega_0 t_n + \theta_0) \tag{2.12}$$

$$\nu_n = b_0\sin(\omega_0 t_n + \theta_0) \tag{2.13}$$

The ML estimate of $\mathbf{a}$ is the value $\hat{\mathbf{a}}$ that maximizes $f(\mathbf{Z};\mathbf{a})$. The maximum of (2.10) occurs a the maximum of $log(f)$ hence the function to be maximized is given by

$$L = -\frac{1}{N}\sum_{n=0}^{N-1}(\mathbf{X}_n-\mu_n)^2+(\mathbf{Y}_n-\nu_n)^2 \tag{2.14}$$

After some simplifications and rearrangements we get

$$L = 2b\,Re[\exp(-j\theta)\exp(-j\omega t_0)A(\omega)] - b^2 \tag{2.15}$$

where

$$A(\omega) = \frac{1}{N}\sum_{n=0}^{N-1} Z_n\, e^{-jn\omega T} \tag{2.16}$$

and $Re[\cdot]$ is the real part of $[\cdot]$. The ML estimate of ω is the value $\hat{\omega}$ which maximizes $A(\omega)$. The estimated amplitude $\hat{b}$ is given by

$$\hat{b} = |A(\hat{\omega})| \tag{2.17}$$

and finally the phase $\hat{\theta}$ can be obtained as

$$\hat{\theta} = \arg\left[A(\hat{\omega})\right] \tag{2.18}$$

where $\arg[\cdot]$ means the argument of $[\cdot]$.

We can observe that Equation (2.16) is similar to the discrete-time Fourier transform of the complex vector $\mathbf{Z}$ which is defines as

$$A_k = \frac{1}{N}\sum_{n=0}^{N-1} Z_n\, e^{-j\frac{2\pi nk}{N}} \qquad \text{for} \quad k = 0, 1, ..., N-1 \tag{2.19}$$

Hence the DTFT can be used to estimate the signal parameters. In [12] the analogy of the two methods is deeply analyzed. By compering (2.19) with (2.16), it appears that the DTFT represents a sampled version of the ML, therefore can be used for a rough estimation. The ML can be computationally expensive and since fast algorithm are available for the DTFT, this approach can be preferred. The accuracy of both, the ML and DTFT, depends on the observation time [12], which means the longer is the observation period the better is the accuracy of the estimate. On the other hand, having longer observation implies larger averaging that can decrease the accuracy in a dynamic case; therefore a trade-off has to be considered for a real and practical working system.

2.2.2 Phase Locked Loop

In this section the PLL is introduced, described and analyzed, starting from the analog model up to the design and development of the discrete version used in the software implementation for testing its capability.

The PLL is a system architecture used for synchronizing oscillator at the receiver side, which is typically asynchronous respect to the transmitter one [13]. They are also used to synchronize the data symbol (symbol timing) but

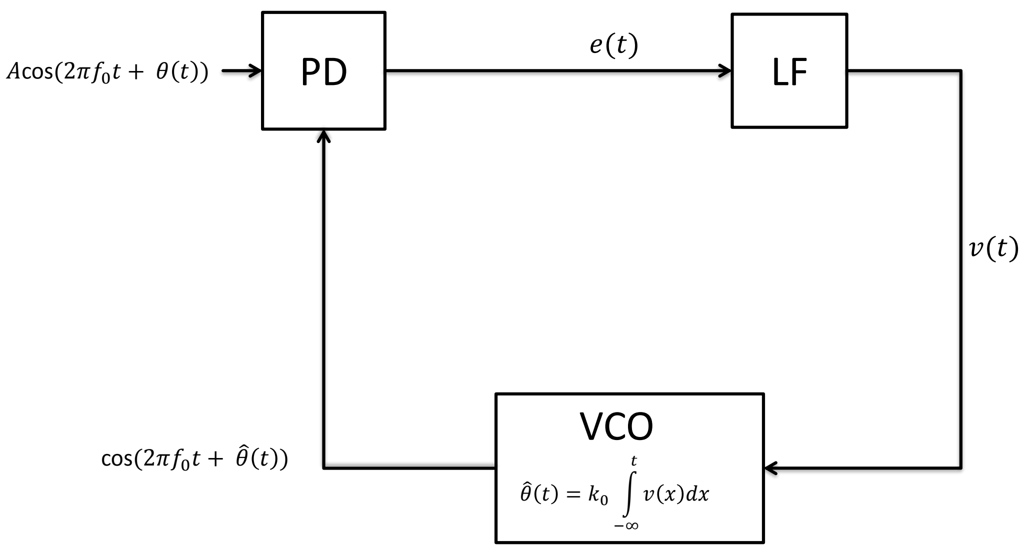

FIGURE 2.2: General block diagram for a PLL with the three main blocks (PD, LF, VCO)

in this case it is used to obtain ranges. The PLL is able to track the phase and the frequency (with relatively small deviation) of a CW. The general block diagram of an analog PLL is depicted in Figure 2.2, where its three main blocks are represented:

1. the phase detector (PD);
2. the loop filter (LF);
3. the voltage controlled oscillator (VCO).

We start assuming that the input signal is a pure sinusoidal signal with amplitude A, frequency f_0 and phase θ, as [13]

$$s_i(t) = A\cos(2\pi f_0 t + \theta(t)) \tag{2.20}$$

The PD is a device that extracts the phase difference between the input incoming signal and the output signal replica generated by the VCO as follows

$$s_{VCO}(t) = \cos(2\pi f_0 t + \hat{\theta}(t)) \tag{2.21}$$

The PD generates an error signal $e(t)$ which depends on the phase error and, typically, this is a non linear function of the phase error which makes the system nonlinear. Then, the error signal is filtered by the LF which has a key role in determining the behavior of the PLL and it is accurately analyzed in Section 2.2.2.1. Finally, the filtered signal is provided to the VCO which will drive the frequency (and the phase) in order to lock on the input signal frequency (and the phase). The VCO is represented as an integrator in the Figure 2.2, in fact it integrates the phase variation respect to time or equivalently the frequency. The estimated phase can be written as

$$\hat{\theta}(t) = k_0 \int_{-\infty}^{t} v(x)dx \tag{2.22}$$

where k_0 is the VCO gain and $v(x)$ the filtered error signal.

Let's assume now that the phase detector is based on a simple multiplier and the input is a sinusoidal signal, hence its output is [14]

$$\begin{aligned} e(t) &= A\sin(2\pi f_0 t + \theta(t))\cos(2\pi f_0 t + \hat{\theta}(t)) \\ &= \frac{A}{2}\left[\sin(\theta(t) - \hat{\theta}(t)) + \sin(4\pi f_0 t + \theta(t) + \hat{\theta}(t))\right] \end{aligned} \tag{2.23}$$

The higher order frequency term will be filtered by the LF, when properly designed, therefore the error signal can be written as

$$e(t) = \frac{A}{2}\sin(\theta(t) - \hat{\theta}(t)) \tag{2.24}$$

which is a non linear function of the phase error. Moreover, it depends on the amplitude A of the input signal and it is important to say that this is true only if the same frequency f_0 is used.

Clearly, the system is a non linear feedback control system. However, it can be analyzed by linearizing it around the desired working point[13]. The desired working point is $\theta_e = \theta - \hat{\theta} = 0$ and, for small variation around it, the small angle assumption is valid therefore

$$\sin(\theta_e(t)) \approx \theta_e(t) \tag{2.25}$$

and $e(t)$ can be approximated as follows

$$e(t) \approx \frac{A}{2}\theta_e(t) \tag{2.26}$$

After the linearization, the system can be analyzed in the Laplace domain. The system block diagram of the phase equivalent model is depicted in Figure 2.3. and its transfer function is given by [13]

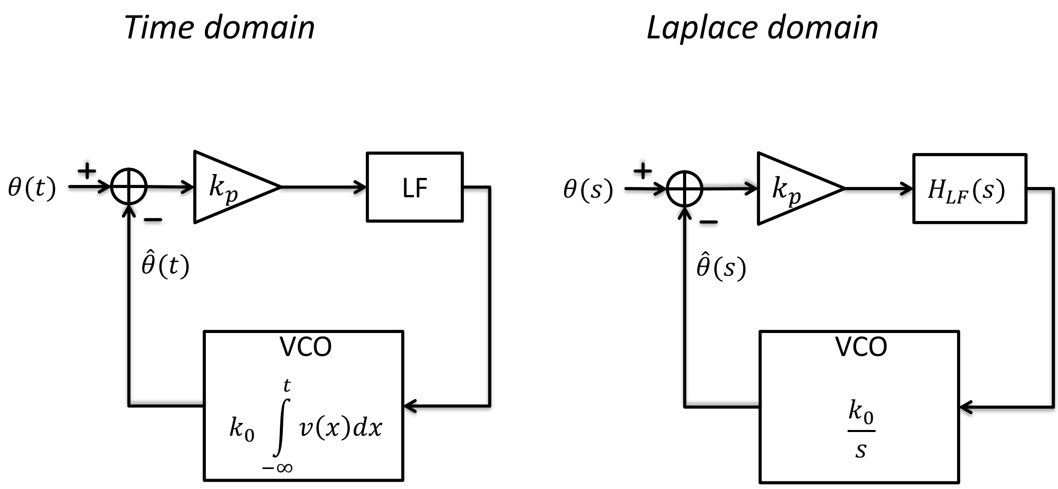

FIGURE 2.3: Left: time domain PLL phase equivalent block diagram. Right: Laplace domain PLL phase equivalent block diagram

$$H(s) = \frac{\hat{\theta}(s)}{\theta(s)} = \frac{k_p k_0 H_{LF}(s)}{s + k_p k_0 H_{LF}(s)} \tag{2.27}$$

where $H_{LF}(s)$ is the transfer function of the loop filter while k_p and k_0 are the PD and VCO gains respectively. The order of the PLL is given by the order of the denominator of (2.27) which depends on the loop filter transfer function.

In general, it can be seen that the order of the PLL is

$$N_{PLL} = N_{LF} + 1 \tag{2.28}$$

where N_{LF} is the order of the loop filter whereas the plus one is due to the VCO (always of order 1).

Of particular relevance is the phase error transfer function that is given by [13]

$$H_e(s) = \frac{\theta_e(s)}{\theta(s)} = \frac{s}{s + k_p k_0 H_{LF}(s)} \tag{2.29}$$

In fact, equation (2.29) is important to analyze the phase error response of the PLL respect to different types of input signal.

2.2.2.1 The Loop Filter

The loop filter plays the key role in the behavior of the PLL, in fact the phase error response depends mainly on the choice of this component. Let's assume that the general transfer function of the loop filter is represented by [13]

$$H_{LF}(s) = \frac{a_1 s + a_0}{b_1 s + b_0} \tag{2.30}$$

Three different filters can be defined as follows by changing the coefficients a_0, a_1, b_0 and b_1:
Case 1 $a_1 = b_2 = 0$ it is a simple gain

$$H_{LF_1}(s) = k \tag{2.31}$$

Case 2 $a_1 = 0$ it is a low pass filter

$$H_{LF_2}(s) = \frac{k}{s + k} \tag{2.32}$$

Case 3 $b_0 = 0$ it is the proportional plus integrator (PI) filter

$$H_{LF_3}(s) = k1 + \frac{k2}{s} \tag{2.33}$$

By substituting (2.31), (2.32) and (2.33) in (2.29), it is possible to analyze the steady-state phase error of the PLL to diverse input. The input considered are [15]:

1) Phase Step: the input is a phase step function ($u(t)$) with size $\Delta\theta$

$$\theta(t) = u(t)\Delta\theta \tag{2.34}$$

and in the Laplace domain

$$\theta(s) = \frac{\Delta\theta}{s} \tag{2.35}$$

2) Frequency Step or Phase Ramp: the input is a frequency step with size Δf or equivalently a phase ramp

$$\theta(t) = 2\pi\Delta f t \tag{2.36}$$

and in the Laplace domain

$$\theta(s) = \frac{2\pi\Delta f}{s^2} \tag{2.37}$$

3) Frequency Ramp of Phase Hyperbola: the input is a frequency ramp with a rate of change $\Delta\dot{f}$ or equivalently a phase hyperbola

$$\theta(t) = 2\pi\Delta\dot{f}\frac{t^2}{2} \tag{2.38}$$

and in the Laplace domain

$$\theta(s) = \frac{2\pi\Delta\dot{f}}{s^3} \tag{2.39}$$

The steady-state phase error is obtained by using the final value theorem [16]

$$\lim_{t\to\infty} f(t) = \lim_{s\to 0} sF(s) \tag{2.40}$$

hence

$$\theta_e(\infty) = \lim_{s\to 0} sH_e(s)\theta(s) \tag{2.41}$$

and the results for the filters and input mentioned earlier are summarized in the Table 2.1, from which we can deduce that the PI filter gives the optimal performance in terms of steady-state phase error. The PI filter is able to track a frequency step with zero phase error and the frequency ramp also called jerk (due to the fact that it is typically induced by acceleration) with a phase error that is non zero. On the opposite, the other filters are characterized by non zero phase error for the frequency step (induced by Doppler effect) and they can not track the frequency ramp which results in the divergence of the phase estimate. Therefore, this is the reason behind the choice of the PI filter for the R-Mode PLL that is described in Section 3

Other filters, with higher order, might be used, and typically the higher is the order of the PLL the better are performance in terms of ability to follow signal variation. For example, a third order PLL can track a frequency ramp with zero phase error, feature that becomes peculiar in application with high dynamic condition (e.g. GNSS). On the other hand the complexity of the design increases with the increase of the order and given that in our scenario the Doppler is limited , as described in Section 3.2, the choice of the PI filter is

Filter		Input		
Name	$H_{LF}(s)$	$\Delta\theta$	Δf	$\Delta\dot{f}$
P	k	0	$\frac{2\pi\Delta f}{k_0 k_p k}$	∞
I	$\frac{k}{s+k}$	0	$\frac{2\pi\Delta f}{k_0 k_p}$	∞
PI	$k1+\frac{k2}{s}$	0	0	$\frac{2\pi\Delta\dot{f}}{k_0 k_p k_2}$

TABLE 2.1: Steady-state phase error for three different filters (P, I, PI) and inputs(phase step, frequency step, frequency ramp).

justified.

Consequently only the PLL with a PI filter is considered in the design, however for further details on the other filters the reader may refer to [13], [16] and [15].

2.2.2.2 Transient and Loop Bandwidth

As stated in Section 2.2.2.1, it is assumed that the PLL uses the PI filter, hence the transfer function of the phase equivalent model is the following

$$H_{PLL}(s) = \frac{k_0 k_p k_1 s + k_0 k_p k_2}{s^2 + k_0 k_p k_1 s + k_0 k_p k_2} \tag{2.42}$$

Equation (2.42) can be written as

$$H_{PLL}(s) = \frac{2\zeta\omega_n s + {\omega_n}^2}{s^2 + 2\zeta\omega_n s + {\omega_n}^2} \tag{2.43}$$

where

$$\zeta = \frac{k1}{2}\sqrt{\frac{k_0 k_p}{k_2}} \tag{2.44}$$

is the so called **damping factor** and

$$\omega_n = \sqrt{k_0 k_p k_2} \tag{2.45}$$

is called **natural frequency**. The response of the loop depends on these two parameters thence by changing them we can change the behavior of the PLL.

The poles of the transfer function are given by

$$p_1, p_2 = -\zeta\omega_n \pm \omega_n\sqrt{\zeta^2 - 1} \quad (2.46)$$

and three different cases are possible[13]:

1. **Underdamped system**: in this case $\zeta < 0$ and the system is called underdamped. The poles are complex conjugate pairs and the response exhibits damped oscillation in the time domain.

2. **Critically damped system**: in this case $\zeta = 1$ and the system is called critically damped. The pole is real with multiplicity two (the two poles are equal) and the time response is between a damped oscillation and decaying exponential.

3. **Overdamped system**: in this case $\zeta > 1$ and the system is called overdamped. The poles are real and different and the response follows a decaying exponential.

The effect of the damping factor can be seen in the frequency domain by looking at Figure 2.4 which depicts the magnitude of the frequency response. It is clear that the PLL acts as a low pass filter and the damping factor controls the magnitude of the frequency response especially around $\omega = \omega_n$. It can be observed that for $\zeta < 1$ the response exhibits a peak at roughly $\omega = \omega_n$ which brings to the so called "overshoot" in the time domain [13]. The over shoot is defined in percentage as

$$OS = \frac{y_{max} - x}{x}\% \quad (2.47)$$

where OS is the overshoot in percentage, y_{max} is the peak maximum output and x is the input step command amplitude. An example of the step response in time domain is depicted in Figure 2.5. It can be observed that the overshoot increases by decreasing the damping factor, on the other hand if it is increased, the overshoot decreases. The opposite trend can be seen for the bandwidth which decreases when the damping is increased and vice-versa.

For the stability of the system, it can be noted in (2.46) that the real part of the poles is always in the left part of the S-plane hence the system is inherently stable [17] since it is constraint by $\zeta > 0$ and $\omega_n > 0$.

There is another important feature of the PLL that has to be considered, the so called **equivalent noise bandwidth** B_n. By considering the transfer function of the PLL and applying the substitution $s = j2\pi f$ we can obtain the area of the PLL transfer function magnitude as

$$B_{PLL} = \int_{-\infty}^{\infty} |H_{PLL}(j2\pi f)|^2 df \quad (2.48)$$

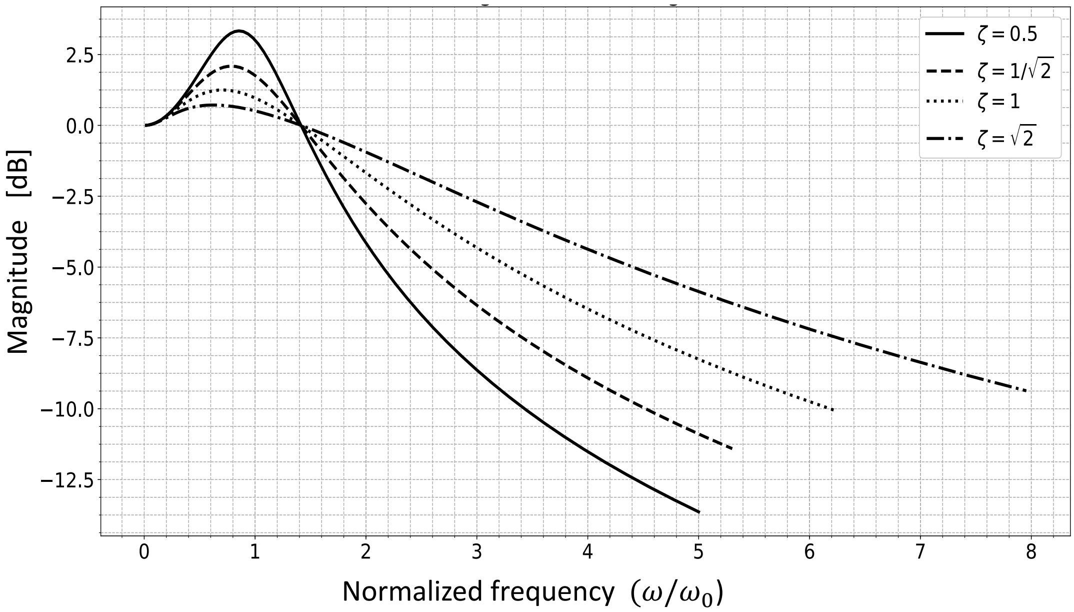

FIGURE 2.4: Frequency impulse response of second order PLL for different values of damping factor

The equivalent noise bandwidth is the bandwidth of an ideal rectangular low pass filter that equates (2.48). In the literature this is given often as a one-side equivalent bandwidth, hence [13]

$$B_n = \frac{1}{2|H_{PLL}(0)|^2} \int_0^\infty |H_{PLL}(j2\pi f)|^2 df \tag{2.49}$$

given in Hertz. For the PI filter the PLL equivalent noise bandwidth can be expressed as

$$B_n = \frac{\omega_n}{2}\left(\zeta + \frac{1}{4\zeta}\right) \tag{2.50}$$

2.2.2.3 Acquisition and Tracking

Acquisition and tracking performance are important features for the PLL. The acquisition is the process that brings the PLL from the unlocked to the locked state. It can be divided in **frequency lock** which is the time needed to steer the frequency of the VCO towards the reference frequency, and **phase lock** that is the time needed to reduce the phase error to the steady state value. A rough

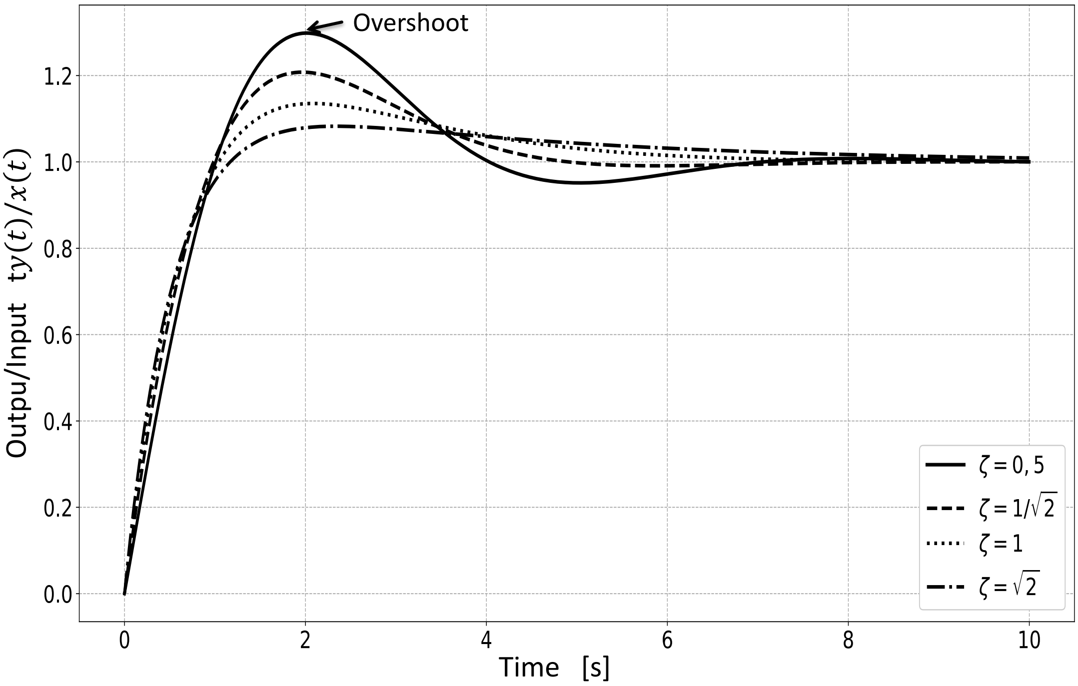

FIGURE 2.5: Time response obtained with a step input for different values of damping factor

estimate of the lock time is given by [15]

$$T_{lock} = T_{phase\ lock} + T_{frequency\ lock} \tag{2.51}$$

where

$$T_{frequency\ lock} \approx 4.2\frac{\Delta f^2}{B_n^3} \tag{2.52}$$

$$T_{phase\ lock} \approx \frac{4}{\omega_n} \tag{2.53}$$

hence

$$T_{lock} \approx \frac{4}{\omega_n} + 4.2\frac{\Delta f^2}{B_n^3} \tag{2.54}$$

By using (2.50), we get ω_n as function of B_n and ζ

$$\omega_n = \frac{2B_n}{\left(\zeta + \frac{1}{4\zeta}\right)} \tag{2.55}$$

and by substituting (2.55) in (2.54) we obtain the lock time as function of B_n and ζ

$$T_{lock} \approx 2\frac{\left(\zeta + \frac{1}{4\zeta}\right)}{B_n} + 4.2\frac{\Delta f^2}{B_n^3} \tag{2.56}$$

The equation (2.56) shows that the lock time decreases if B_n is increased and vice-versa. The equation is valid for a rough estimation of the locking time by using a simple multiplier. When a complex multiplier phase detector is used, which is described in Section 3, the performance are slightly different and in this case a different formula is used, which is derived in [16] for the JK-flipflop PD. In [16] multiple PD_s and loop filters are analyzed and by comparing the S-function of the complex multipliers with the JK-flipflop one (when a PI filter is used) the analogy is clear, hence the locking time formula becomes

$$T_{lock} \approx \frac{2\pi}{\omega_n} + \frac{(2\Delta f)^2}{\zeta\omega_n^2} \tag{2.57}$$

The tracking performance is given by the variance of the phase error which can be expressed as

$$\sigma_{\theta_e}^2 = E\left\{\left|\theta - \hat{\theta}\right|^2\right\} \tag{2.58}$$

where θ is the input signal phase and $\hat{\theta}$ is the estimated phase. Assuming a sinusoidal signal with power P in w and an additive white Gaussian noise (AWGN) with power spectral density $N_0/2$ W/Hz, the variance is given by [13]

$$\sigma_{\theta_e}^2 = \frac{N_0 B_n}{P} \tag{2.59}$$

hence a small bandwidth allows better tracking performance (extremely important four our purposes) by filtering out more noise. On the other hand, by looking at (2.56), the locking time is reduced when the bandwidth is increased, moreover a large bandwidth allows the PLL to track faster variation in the signal (higher Doppler condition). The minimum of B_n for fixed ω_n is given by

$$\frac{\partial B_n}{\partial \zeta} = 0 \tag{2.60}$$

which gives a minimum for $\zeta = \frac{1}{2}$. In this case in fact

$$B_n = \frac{\omega_n}{2} \tag{2.61}$$

The plot of a normalized B_n in function of ζ is represented in Figure (2.6). It can be seen that the values of ζ around 0.5 provide similar bandwidth, therefore a common choice is to set $\zeta = \frac{1}{\sqrt{2}}$ which allows to have a minimum transient [15].

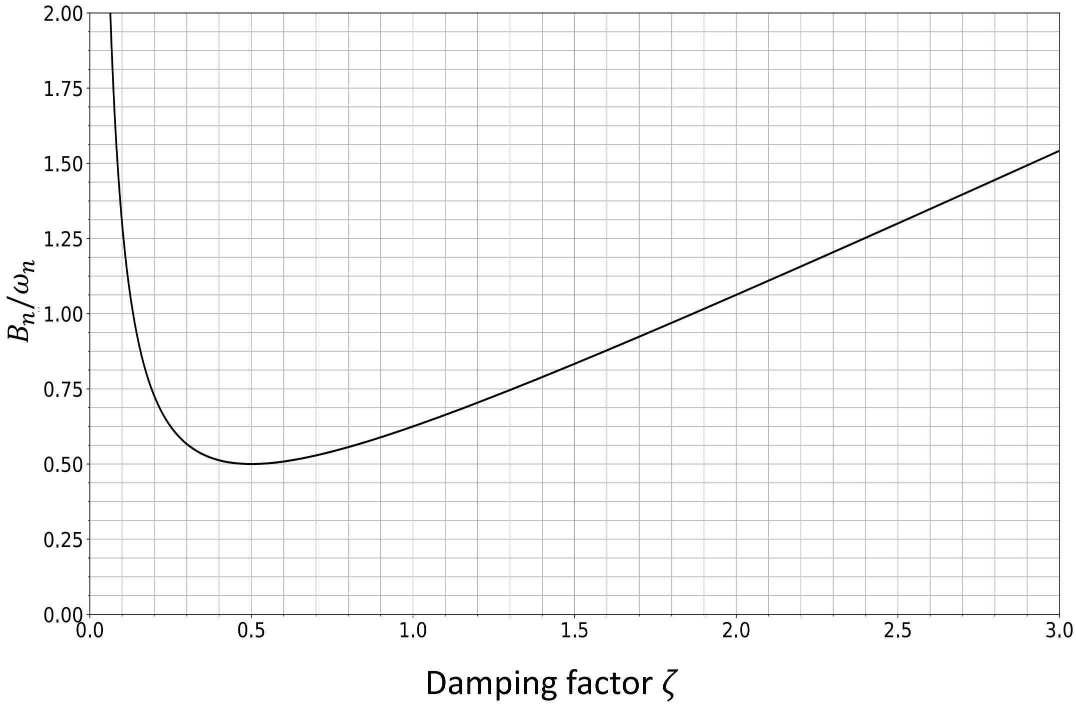

FIGURE 2.6: Noise equivalent bandwidth as function of the damping factor

Chapter 3

PLL Implementation

In the previous sections, the main concepts and the theory related to the PLL, with its fundamental blocks and equations, are introduced. The PLL used for our purpose is based on the analog model with a PI loop filter, which provides the best performance for a second order PLL, therefore the transfer function of the PLL is given by (2.42). However, a different phase detector is adopted, respect to the simple multiplier presented in Section 2.2.2. First of all, the complex signal is used instead of the real signal, thus the input samples are represented by complex numbers with real and imaginary parts. Consequently a complex multiplier is chosen and then the arc-tangent of the imaginary and real part of the signal coming from the complex multiplier is evaluated to obtain a phase error signal. The advantage of using such implementation is that the phase error function becomes linear as shown in the Figure 3.1. It is easy to observe that the function on the right, obtained with the complex multiplier plus the arc-tangent block, is linear, whereas the left one, valid for a simple multiplier, is non linear. Moreover the output signal, which is the correction applied, is equal to the phase error in the range $[-\pi, \pi]$. Another important advantage of the complex multiplier PD is that it is independent of the signal amplitude A while the opposite happens for the simple multiplier. Thanks to this last feature, the usage of an automatic gain control (AGC) system can be avoided. The use of this PD does not affect the transfer function of the PLL that remains the same. A proof that the phase error function is linearly dependent on the phase difference of the input/output signal is given in the following lines.

By assuming that

$$s_i(t) = Ae^{j\theta(t)} \tag{3.1}$$

is the the input signal with amplitude A and phase $\theta(t)$, while

$$s_o(t) = e^{j\hat{\theta}(t)} \tag{3.2}$$

is the output signal with unitary amplitude and estimated phase $\hat{\theta}(t)$. By taking the complex conjugate of $s_o(t)$ and multiply it with $s_i(t)$ we obtain the new

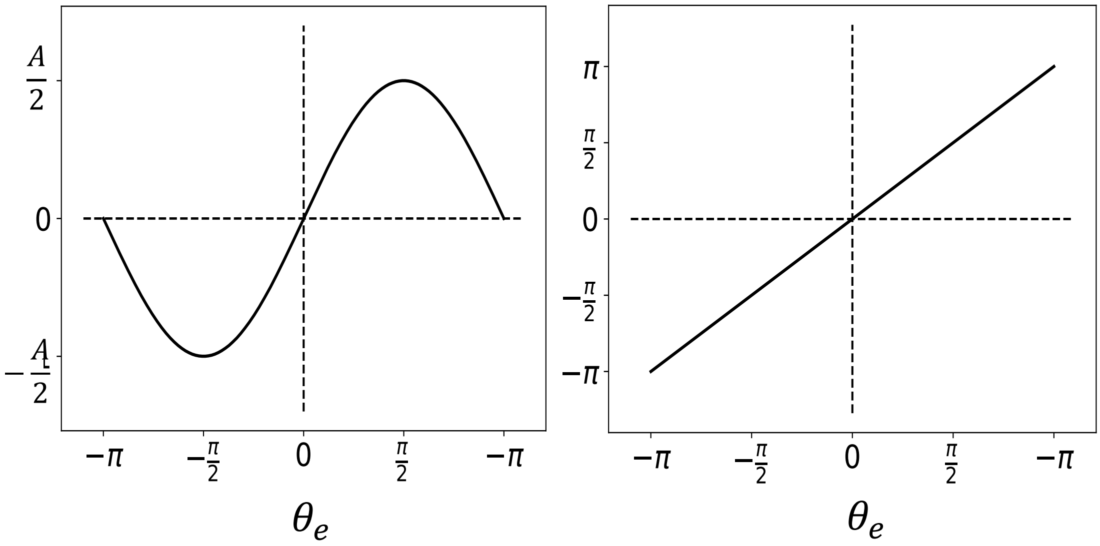

FIGURE 3.1: Left: Phase detector function based on simple multiplier. Right: Phase detector based on the complex multiplier

signal $s(t)$

$$\begin{aligned} s(t) &= s_i(t)\, s_o(t)^* \\ &= Ae^{j\theta(t)} e^{-j\hat{\theta}(t)} \\ &= Ae^{j[\theta(t)-\hat{\theta}(t)]} \\ &= A[\cos(\theta_e(t) + j\sin(\theta_e(t))] \end{aligned} \tag{3.3}$$

The phase error signal $e(t)$ can be obtained with the act-tangent operator as

$$\begin{aligned} e(t) &= tan^{-1}\left\{\frac{\text{Im}[s(t)]}{\text{Re}[s(t)]}\right\} \\ &= \tan^{-1}\left\{\frac{A\sin[\theta_e(t)]}{A\cos[\theta_e(t)]}\right\} \end{aligned} \tag{3.4}$$

hence

$$e(t) = \theta_e(t) \tag{3.5}$$

Equation (3.5) shows that the error function is linear and exactly equal to the phase error hence the PD gain (k_p) does not depend on the amplitude A and assumes the value of 1.

As stated before, the PLL is based on the analog model, which is defined for a continuous time domain. However, a discrete-time version is needed since the goal is to obtain a software defined PLL (SDPLL) which is supposed to work within a sampled data system. Therefore, the PLL is supposed to be part of a software defined radio (SDR) receiver written in Python which will provide the estimated ranges to the user. In the next section, the discrete-time PLL, based on the continuous-time version, is derived.

3.1 Discrete-Time PLL

In this chapter is described the derivation of a discrete-time version of the PLL that behaves like the analog one. The following derivation of the discrete-time PLL is deeply described in [14] and [13], thus here we try to give a short statement of the main steps to derive it.

The starting point is the analog model of the second order PLL obtained by using the PI filter. The equivalent phase model was presented in Figure 2.3 and the transfer function in (2.42) and (2.43).

Secondly, the Bilinear transformation is applied to the analog transfer function in order to obtain a discrete-time transfer function in the z-domain. By substituting $s = \frac{T}{2}\frac{1+z^{-1}}{1-z^{-1}}$ in (2.43) where T is the sampling time, we obtain

$$H_{PLL}\left(\frac{T}{2}\frac{1+z^{-1}}{1-z^{-1}}\right) = \frac{2\zeta\omega_n(\frac{T}{2}\frac{1+z^{-1}}{1-z^{-1}}) + {\omega_n}^2}{(\frac{T}{2}\frac{1+z^{-1}}{1-z^{-1}})^2 + 2\zeta\omega_n(\frac{T}{2}\frac{1+z^{-1}}{1-z^{-1}}) + {\omega_n}^2} \tag{3.6}$$

and after some mathematical manipulations [14]

$$H_{PLL}\left(\frac{T}{2}\frac{1+z^{-1}}{1-z^{-1}}\right) = \frac{\frac{2\zeta\theta_n+\theta_n^2}{1+2\zeta\theta_n+\theta_n^2} + 2\frac{\theta_n^2-\zeta\theta_n}{1+2\zeta\theta_n+\theta_n^2}z^{-1} + \frac{\theta_n^2}{1+2\zeta\theta_n+\theta_n^2}z^{-2}}{1 - 2\frac{\theta_n^2-1}{1+2\zeta\theta_n+\theta_n^2}z^{-1} + \frac{1-2\zeta\theta_n+\theta_n^2}{1+2\zeta\theta_n+\theta_n^2}z^{-2}} \tag{3.7}$$

where

$$\theta_n = \frac{\omega_n T}{2} \tag{3.8}$$

At this point, a digital implementation of the PLL that emulates the analog one is required. The Figure 3.2 shows the block diagram of the phase equivalent digital PLL and its transfer function in the z-domain is

$$H(z) = \frac{K_pK_0(K_1+K_2)z^{-1} - K_pK_0K_1z^{-2}}{1 - 2(1 - \frac{1}{2}K_pK_0(K_1+K_2))z^{-1} + (1 - K_pK_0K_1)z^{-2}} \tag{3.9}$$

where K_p and K_0 are the gains of the digital PD and the numerically controlled oscillator (NCO) whereas K_1 and K_2 are the PI filter gains. By equating the denominators in 3.9 and 3.7 and comparing the z^{-1} and z^{-2} terms we get

$$1 - \frac{1}{2}K_pK_0(K_1 + K_2) = \frac{\theta_n^2 - 1}{1 + 2\zeta\theta_n + \theta_n^2} \tag{3.10}$$

and

$$1 - K_pK_0K_1 = \frac{1 - 2\zeta\theta_n + \theta_n^2}{1 + 2\zeta\theta_n + \theta_n^2} \tag{3.11}$$

By solving (3.11) and (3.10) for $K_pK_0K_1$ and $K_pK_0K_2$

$$K_pK_0K_1 = \frac{4\zeta\theta_n}{1 + 2\zeta\theta_n + \theta_n^2} \tag{3.12}$$

$$K_pK_0K_2 = \frac{4\theta_n^2}{1 + 2\zeta\theta_n + \theta_n^2} \tag{3.13}$$

Recalling equation (2.50), θ_n can be expressed as a function of the damping factor ζ and the noise equivalent bandwidth B_n

$$\theta_n = \frac{B_nT}{\zeta + \frac{1}{4\zeta}} \tag{3.14}$$

hence substituting in (3.12) and (3.13)

$$K_pK_0K_1 = \frac{4\zeta\left(\frac{B_nT}{\zeta+\frac{1}{4\zeta}}\right)}{1 + 2\zeta\left(\frac{B_nT}{\zeta+\frac{1}{4\zeta}}\right) + \left(\frac{B_nT}{\zeta+\frac{1}{4\zeta}}\right)^2} \tag{3.15}$$

$$K_pK_0K_2 = \frac{4\left(\frac{B_nT}{\zeta+\frac{1}{4\zeta}}\right)^2}{1 + 2\zeta\left(\frac{B_nT}{\zeta+\frac{1}{4\zeta}}\right) + \left(\frac{B_nT}{\zeta+\frac{1}{4\zeta}}\right)^2} \tag{3.16}$$

Equations (3.15) and (3.16) are then used to obtain the gains of the discrete-time PLL, which will behave like the analog version with fixed damping factor and the equivalent noise bandwidth.

Typically, the NCO gain K_0 is set to be one and the gain K_p for the complex multiplier PD is also equal to one, thereafter the PLL depends on the PI filter gains K_1 and K_2

$$K_1 = \frac{4\zeta\left(\frac{B_nT}{\zeta+\frac{1}{4\zeta}}\right)}{1 + 2\zeta\left(\frac{B_nT}{\zeta+\frac{1}{4\zeta}}\right) + \left(\frac{B_nT}{\zeta+\frac{1}{4\zeta}}\right)^2} \tag{3.17}$$

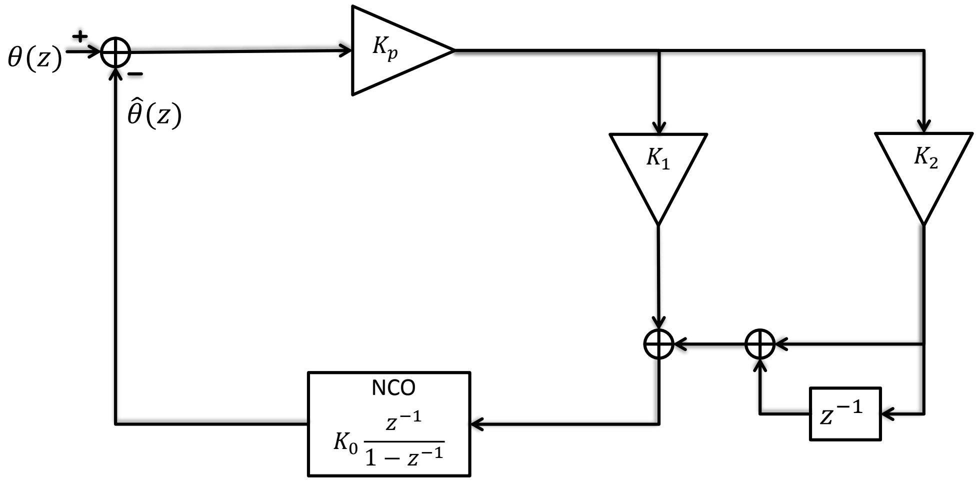

FIGURE 3.2: Digital PLL equivalent phase PLL.

$$K_2 = \frac{4\left(\frac{B_n T}{\zeta+\frac{1}{4\zeta}}\right)^2}{1+2\zeta\left(\frac{B_n T}{\zeta+\frac{1}{4\zeta}}\right)+\left(\frac{B_n T}{\zeta+\frac{1}{4\zeta}}\right)^2} \tag{3.18}$$

The complete block diagram of the discrete-time PLL is given in Figure 3.3. It is clear that there are three main blocks as for the continuous-time PLL. Easily, it can be seen that the VCO is replaced by a different device which is called numerically controlled oscillator which is used to generate a precise reference frequency in software. The model in Figure 3.3 is implemented in Python in order to have a software defined PLL and by looking at the picture we can observe that three parameters need to be set:

1. The filter gains K_1 and K_2
2. The quiescent frequency μ_0 of the NCO, which represents the natural frequency of the clock which, in this case, is the reference frequency of the signal that will be tracked by the PLL

The filter gains are set by using 3.17 and 3.18 , while for the quiescent frequency μ_0 it can be used the following

$$\mu_0 = \frac{2\pi f_0}{f_s} \tag{3.19}$$

where f_0 is the reference signal frequency we want to track and f_s is the sampling frequency.

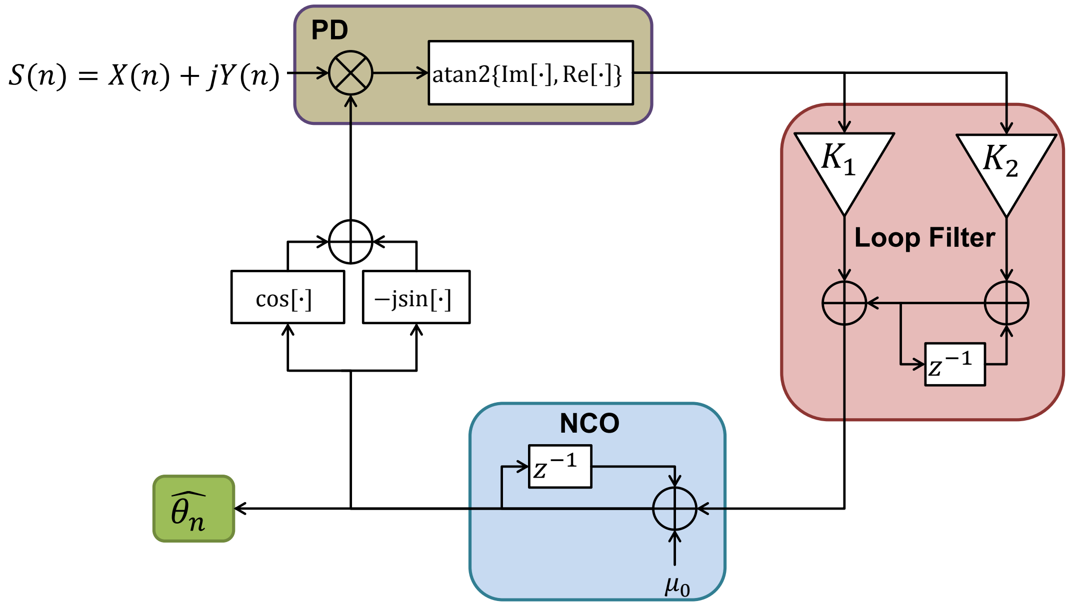

FIGURE 3.3: Discrete-time PLL.

3.2 Parameter Selection

In the previous section we derived the discrete-time PLL model used for implementing our software defined PLL with the parameters that need to be set. Selecting the parameters is not an easy task given that several effects need to be taken into account (required accuracy, lock time, phase noise, overshoot), so we start with the assumption that

$$\zeta = \frac{1}{\sqrt{2}} \tag{3.20}$$

which is a good choice in order to get small transient effect, as shown in Section 2.2.2.3. By considering the fact that the transmitters are fixed in the position, the Doppler will depend only on the vessel movements, therefore assuming that the maximum speed of a vessel is

$$v_{max} = 30\ m/s \tag{3.21}$$

the maximum Doppler frequency shift is

$$f_{d_{max}} = f_{max} \frac{\pm v_m ax}{c_0} \approx \pm 0.0325\ Hz \tag{3.22}$$

where $f_{d_{max}}$ is the Doppler frequency shift, $f_{max} = 325000$ Hz is the maximum frequency of the signal assumed to be at the upper edge of the system band, as described in Section 1.3 (overestimated choice) whereas c_0 in m/s is the speed of light. Equation (3.22) implies that the Doppler shift increases linearly with the frequency, hence the reason of considering the maximum frequency within the bandwidth. By using (2.59), we can obtain a noise equivalent bandwidth for the PLL by setting a minimum performance requirement on the standard deviation of the phase estimate. We consider the following formula

$$\sigma_{\theta_m} = \sigma_{\theta_e} \frac{c_0}{2\pi f} \tag{3.23}$$

where σ_{θ_m} is the standard deviation in meters, σ_{θ_e} the standard deviation of the phase estimate in radians and f the frequency of the signal. By looking at (3.23), it is clear that, by increasing the signal frequency the standard deviation in meters increases, thereafter the upper bound is given by the lowest frequency in the band which is $f = 285500$ Hz (also in this case it is overestimated). From (2.59) we get

$$\theta_e = \sqrt{\frac{N_0 B_n}{P}} \tag{3.24}$$

where N_0 can be obtained as

$$N_0 = \frac{P}{\frac{C}{N_0}} \tag{3.25}$$

By considering the signal-to-noise density ratio $(C/N_0)_{dB}$ in dB-Hz, (3.23) can be finally written as

$$\sigma_m = \sqrt{\frac{B_n}{10^{\left[\left(\frac{C}{N_0}\right)_{dB}/10\right]}}} \frac{c_0}{2\pi f} \tag{3.26}$$

This formula is fundamental for our purposes, in fact we can use it to obtain the desired accuracy of the phase estimate. It can be noted, that in general the accuracy in meters depends on the loop noise equivalent bandwidth, the carrier-to-noise density ratio and the frequency. By fixing B_n and $(C/N_0)_{dB}$ the accuracy increases linearly with the increase of the frequency and in particular for the R-Mode set of frequencies the performance is 12% better when the highest possible in-band frequency is considered respect to the lowest. Clearly, the $(C/N_0)_{dB}$ level is not linearly impacting the accuracy and by increasing it by a factor of 2 the improvements is roughly the 30% whereas by doubling the bandwidth the loss of performance is about 40%. The formula can be used to find an upper bound for B_n by imposing a target standard deviation $\sigma_{m_{TG}}$. For instance

$$\sigma_{m_{TG}} = 5\,m \tag{3.27}$$

Furthermore, by fix the signal-to-noise density ratio

$$\left(\frac{C}{N_0}\right)_{dB} = 30 \tag{3.28}$$

we get

$$B_{n_{max}} = \frac{\sigma_{m_{TG}}{}^2 10^{\left[\left(\frac{C}{N_0}\right)_{dB}/10\right]}}{\left(\frac{c_0}{2\pi f}\right)^2} \approx 0.89\,Hz \tag{3.29}$$

therefore, all the values of noise equivalent bandwidth, for which $B_n < B_{n_{max}}$ is verified, are acceptable and provide at least an accuracy of 5 m (1 sigma). However, in order to achieve a fast lock, the locking time must be considered as constraint. During the first trial in simulation a larger locking time was observed with respect to the theoretical formula (2.57), as described in Section 4. Therefore, in order to have an acceptable locking time (less than 1 minute) it was decided to impose experimentally an upper bound of T_{lock}. By setting

$$T_{lock} < 7s \tag{3.30}$$

and by using (2.57) we can obtain the curve in Figure 3.4 where the intersection among the requirement curve and the bandwidth curve is highlighted. By looking at the picture it easy to see that

$$B_n > 0.4765Hz \tag{3.31}$$

hence a loop bandwidth greater or equal then 0.5 Hz is considered for the tracking of the continuous wave signals. In accordance with the aforementioned constraints, the noise equivalent bandwidth of the PLL can be chosen in the range [0.5, 0.9).

One more aspect to point out is that the frequency rate of change, due to the acceleration of the vessel is negligible, in fact this will last for a limited amount of time. Let us assume that the vessel is not moving and a time $t_0 = 0$ starts accelerating with a constant acceleration $a = 1\frac{m}{s^2}$. The Doppler frequency can be written as

$$f_d(t) = \pm f_{max}\frac{v(t)}{c_0} \tag{3.32}$$

where $v(t) = at$ is the speed of the vessel, hence

$$f_d(t) = \pm f_{max}\frac{at}{c_0} \tag{3.33}$$

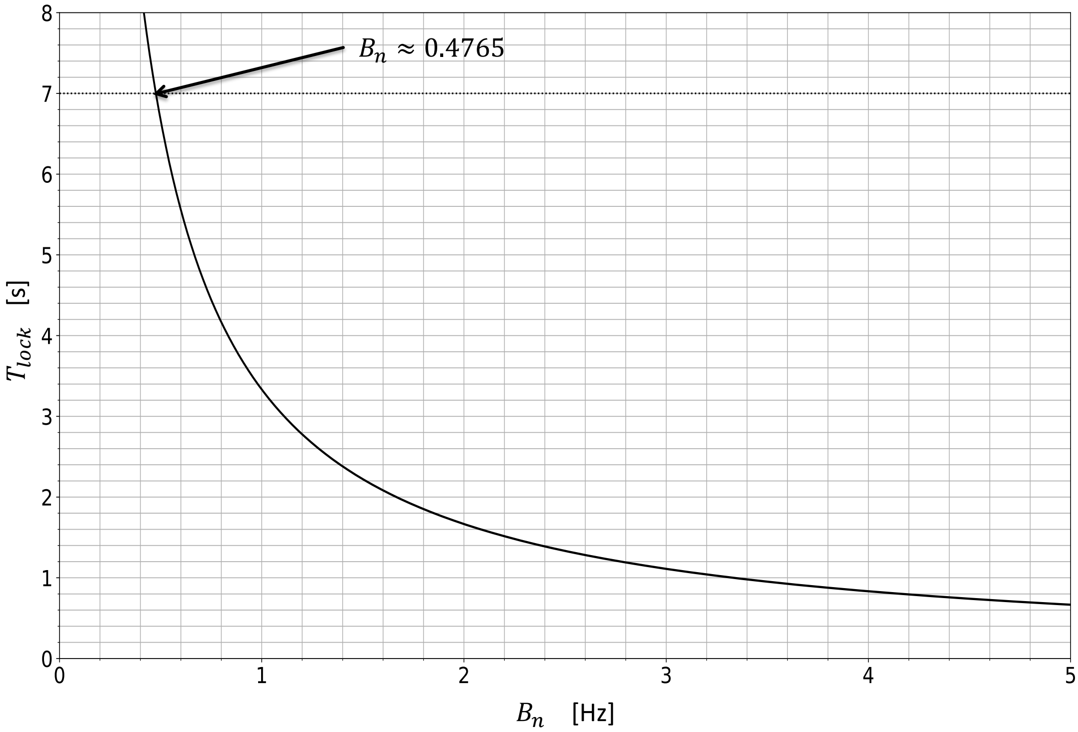

FIGURE 3.4: Plot of the locking time as function of the equivalent noise bandwidth

and the maximum rate of change $\dot{f}_d$ is given by

$$\dot{f}_d = \pm f_{max} \frac{a}{c_0} \approx \pm 0.001084\,\mathrm{Hz/s} \tag{3.34}$$

which is very limited.

Chapter 4

Self-Interference Mitigation

As stated in the section 3.2, the PLL for the CW_s phase tracking is characterized by $\zeta = 1/\sqrt{2}$ and a minimum noise equivalent bandwidth $B_{n_{min}} = 0.5$. An example is depicted in the Figure 4.1, which shows the phase estimate (in

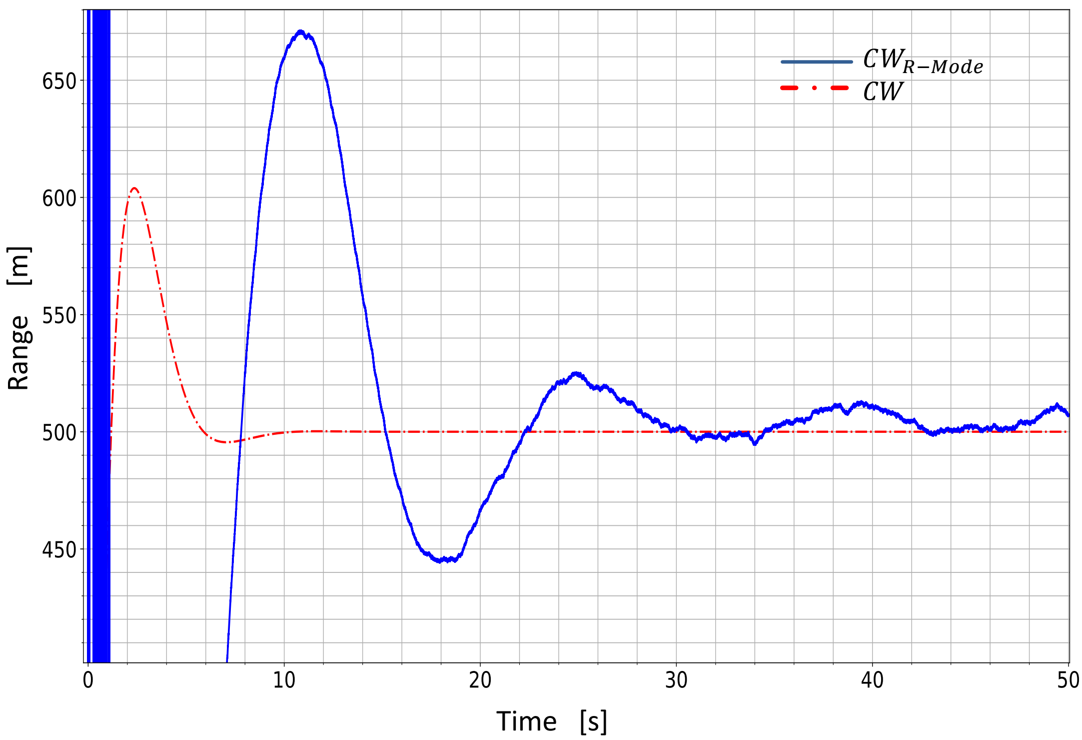

FIGURE 4.1: Estimated phase in meters, in red for the simulated CW signal, while in blue for the simulated R-Mode, both obtained with the same PLL and no noise.

meters) obtained with the PLL introduced in the section 3 by using the aforementioned values of damping factor and noise equivalent bandwidth. On the abscissa axis we have the time in seconds while on the ordinate axis there is the range in meters. The red dashed curve represents the result obtained for a pure continuous wave as input signal while the blue one is the result for the tracking of the lower CW, with the same frequency, of the simulated R-Mode signal. In both the cases there is no noise and it is clear that in case of the R-Mode signal the phase estimation is affected by a degradation of the accuracy due to self-interference effect which is generated by the MSK (mostly) and the other continuous wave. In fact, it can be observed that the phase variance increases and a longer transient is obtained. For these reasons two interference mitigation technique are proposed in section 4.1 and 4.2. The first method is based on the application of multiple PLL cancellation schema while the other is based on the usage of notch filters.

4.1 PLL-based Mitigation

The first approach proposed to cancel out the interference of the MSK and the other continuous wave is based on the PLL architecture. The general idea is that a PLL can be used to track the phase of the MSK signal in order to estimate and remove it. We can divide the process of the interference suppression in three main stages performed in this order:

1. Stage 1: rough tracking of the two continuous wave signals.
2. Stage 2: rough removal of the continuous wave signal in order to start the MSK tracking.
3. Stage 3: tracking of the MSK signal and get rid of it to refine the CW_s phase estimate.

As a first step, we start the PLLs that will estimate the phase of the continuous wave signals. The amplitudes of the two CW are also estimated and this is explained later. Secondly, after the transient, if the estimate is good enough, it can be used to remove most of the two continuous wave signals from the incoming one, allowing a third PLL, with a suitable noise bandwidth, to start working and tracking the MSK. For this PLL, a proper bandwidth needs to be set to accommodate the frequency hops of the MSK modulation scheme. Afterward, for this third PLL some time is required for expiring the transient and suddenly the MSK estimation can be used to subtract itself from the main incoming signal. This cancellation scheme will remove most of the interferent MSK signal allowing the PLL_s running on the CW_s to refine their phase estimation, leading to better accuracy. A graphical explanation of the PLL-based approach is given in Figure 4.2, where we can see the three main stages with the block diagram.

So far, the implementation of the PLL that estimate the phase of the signal was illustrated. However in this approach the amplitude of CW_s and MSK has

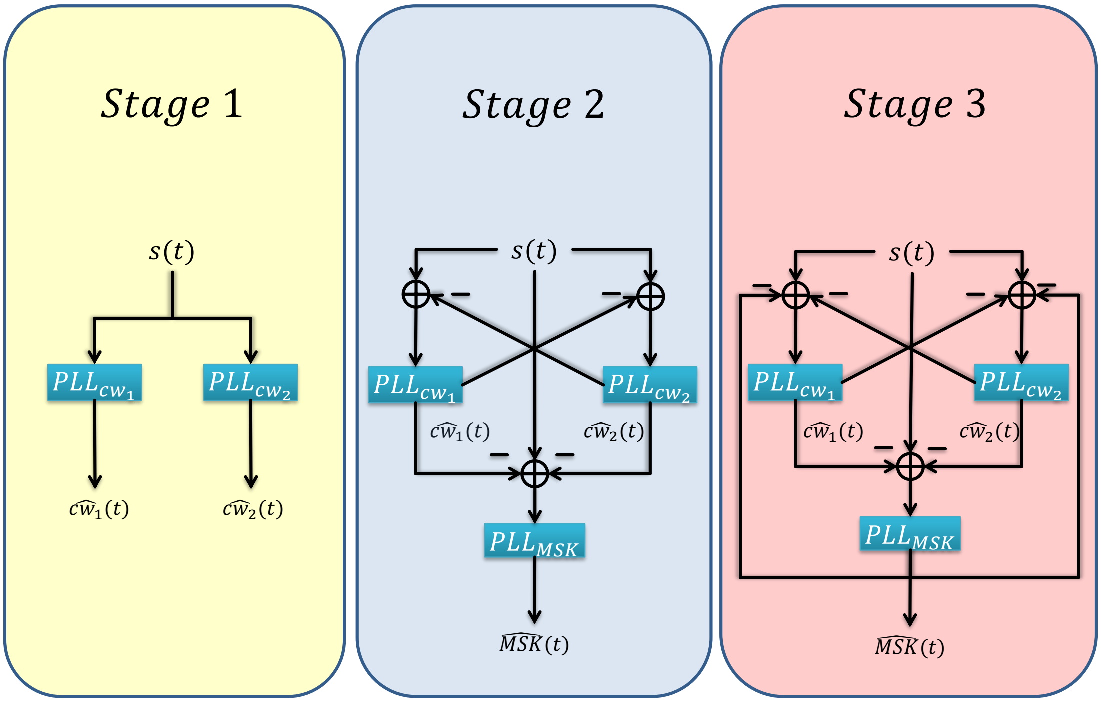

FIGURE 4.2: Three stages of the PLL-based mitigation technique

relevance. For this reason, an amplitude estimation is also needed to properly estimate and remove the signal components. The Figure 4.3 illustrate the architecture used for the estimation of the CW_s and MSK. The PLL tracks the phase of the input signal s which is used to obtain a complex signal with the same phase and unitary amplitude. After the conjugate operation, the multiplication between the input and the obtained signal is performed and the real part of the result is low pass filtered (to filter out the noise). This output $\hat{A}$ is the estimate of the amplitude A that is multiplied with $e^{(j\hat{\theta})}$ to reconstruct the reference input. Supposing that the PLL is already in the lock state we have

$$\theta \approx \hat{\theta} \Rightarrow \theta - \hat{\theta} \approx 0 \tag{4.1}$$

so that

$$Ae^{j\theta}\left(e^{j\hat{\theta}}\right)^{*} = Ae^{j\theta}\left(e^{-j\hat{\theta}}\right) = Ae^{j(\theta-\hat{\theta})} \tag{4.2}$$

and by considering the real part we obtain

$$\mathrm{Re}\left\{Ae^{j(\theta-\hat{\theta})}\right\} \approx \mathrm{Re}\left\{Ae^{j(0)}\right\} = \mathrm{Re}\left\{A[\cos(0) + j\sin(0)]\right\} = A \tag{4.3}$$

The amplitude estimation depends on the state of the PLL, on the contrary the amplitude estimate will not directly affect the PLL. Nevertheless, the estimated signal will be feedback to the other loops and this can compromise the stability of the system in case one of them lose the lock.

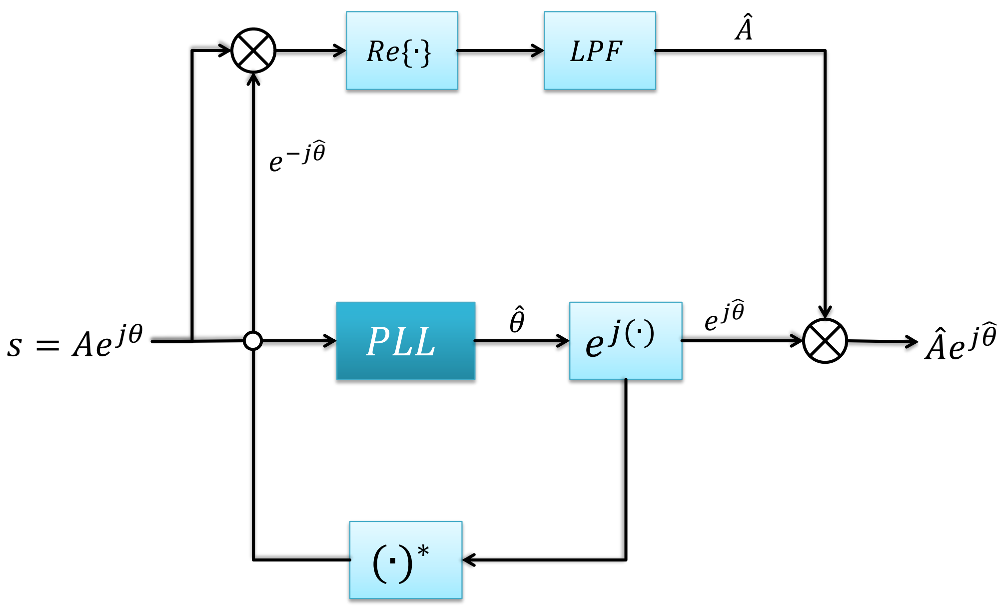

FIGURE 4.3: Block diagram used for signal estimation that is exploited as interference suppression

In this method it is important to set an appropriate noise equivalent bandwidth for the MSK signal which has to be processed by a PLL with different parameters. It is fundamental in fact to consider that the MSK is characterized by jumps in the frequency when there is a change in the bit information. Potentially, the signal can exhibits a jump of ± 50 Hz every 0.01 seconds hence it is needed that the PLL can be able to track such variation in the frequency. Moreover the locking time due to frequency step variation needs to be much smaller than 0.01 s in order to keep the system working properly. For these reasons, by following a similar approach used in Section 3.2, we set

$$T_{lock} < 0.001s \tag{4.4}$$

and by using 2.57 we can obtain the curve in Figure 4.4. It easy to see that

$$B_n > 3333Hz \tag{4.5}$$

in order to satisfy the requirement, therefore to be more robust, since it is based on approximation, it is considered $B_n = 3500$ Hz which will assure an acceptable locking time .

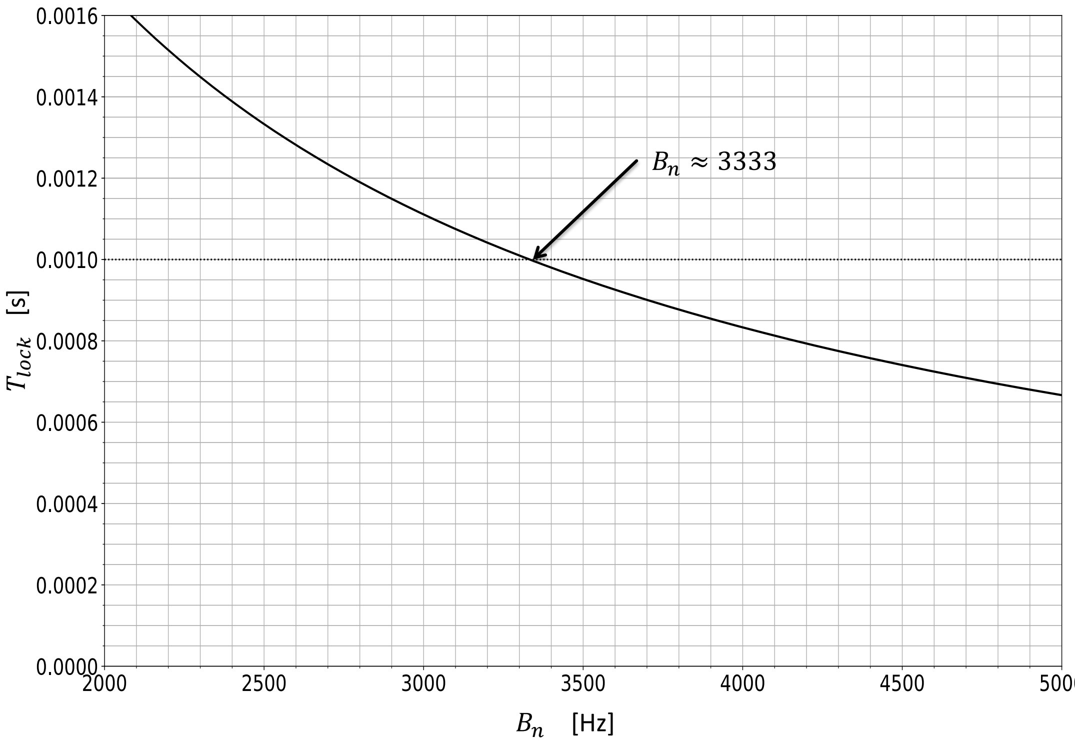

FIGURE 4.4: Plot of the locking time in function of the equivalent loop bandwidth

4.2 Notch Filter Approach

Notch filters have been largely used in GNSS domain to counteract interference generated by CWs [18]. The notch filter used in our approach is an infinite impulse response (IIR) filter described by the following transfer function in the z domain [19]

$$H(z) = \frac{1 - z_0 z^{-1}}{1 - k_\alpha z_0 z^{-1}} \tag{4.6}$$

where z_0 is the complex zero which represents the frequency we want to suppress while k_α is called pole contraction factor. The pole and the zero of the filter are located on the same radial vector of the z-plane. The zero lies on the unitary circle of the plane and can be set by using (4.7)

$$z_0 = e^{j2\pi f_0 T_s} \tag{4.7}$$

where f_0 is the frequency to cancel out in Hz and T_s is the sampling time in seconds, while the pole location depends on k_α, with $0 \leq k_\alpha < 1$. The pole contraction factor plays a key role, in fact the width of the filter depends on that parameter [18]. An example is shown in the Figure 4.5, where we can easily see the difference in the magnitude and phase diagram with a different contraction factor. For a better understanding, also the R-Mode normalized spectrum is plotted in red dashed line. The left side of Figure 4.5 is obtained by using $z_0 = 299,775\ kHz$ and $k_\alpha = 0.99$ while for the right side z_0 is the same but the contraction factor is $k_\alpha = 0.9999$. It is possible to observe that by increasing the contraction factor ($k_\alpha - > 1$) the bandwidth of the filter is narrowed, hence the CW is filtered without impacting the remaining part of the signal in a relevant manner. On the contrary if it is decreased the bandwidth is broadened which means that the other frequencies are affected by the filtering process. By setting the appropriate parameters, the continuous wave

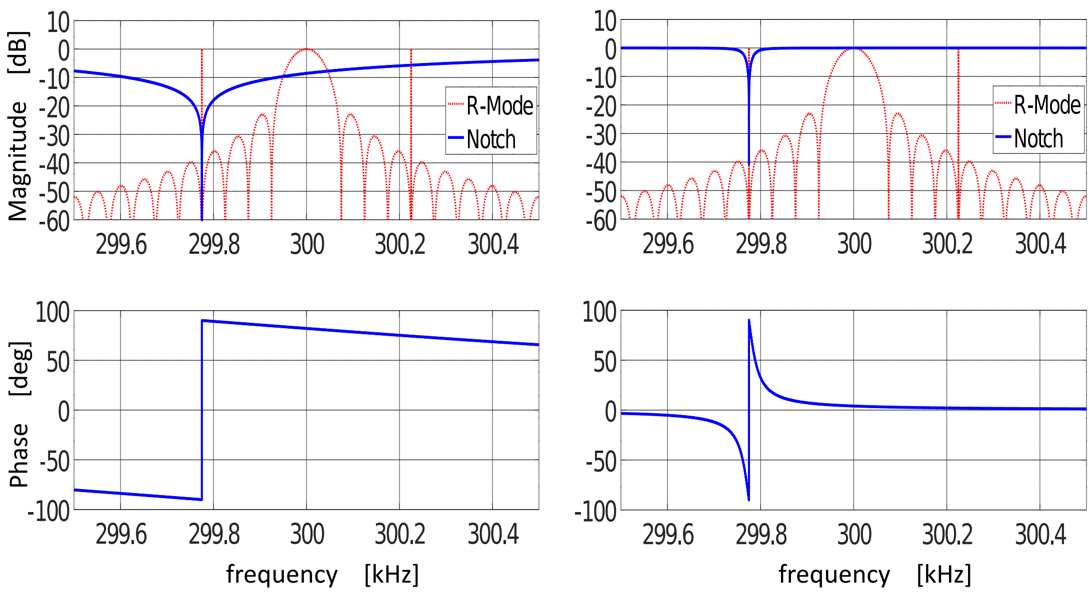

FIGURE 4.5: Bode diagrams: at the top the magnitude, at the bottom the phase. The dotted red line represent the R-Mode normalized spectrum while the blue line represents the notch filter. On the left side $k_\alpha = 0.99$ while on the right side $k_\alpha = 0.9999$ and in both cases $z_0 = 299,775\ kHz$.

can be filtered out and the output filtered signal will contain only the MSK and the other CW. Afterwards, this filtered signal can be subtracted to the main input signal, obtaining a clean version of the reference CW which can be tracked by the PLL. The mitigation scheme is based on this principle and it is shown in Figure 4.6. Three branches are depicted, the first one is tracking the CW_1, the second is tracking the CW_2 while the third branch can track the MSK. Of particular importance are the branches one and two, that we want to use for obtaining ranges whereas the third one can be used for further processing reasons. The delay block z^{-1} is used for synchronization purpose, in fact without

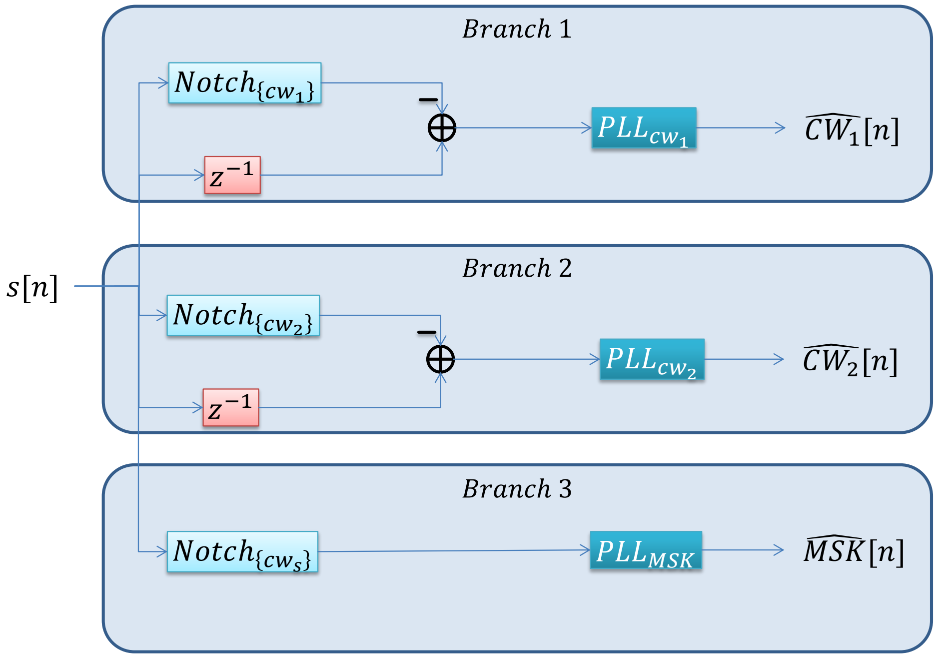

FIGURE 4.6: Notch filter mitigation approach: the three branches are independent of each other

that block the output of the notch filter and the incoming signal $s[n]$ would be shifted by one sample respect to each other.

In this approach the contraction factor is set in order to be insensitive to the Doppler effect and to avoid distortion of the MSK and the other CW. We already said that increasing the contraction factor a narrower filter is obtained, however in case of a frequency shift (e.g. Doppler) the notch filter pole and the signal frequency are not matching anymore. Therefore, this will impact on the performance of the mitigation schema. Assuming the same condition as in Section 3.2, where the maximum speed of the vessel is assumed to be 30 m/s, the maximum Doppler frequency for a reference CW with frequency 325000

Hz is

$$f_d \approx \pm 0.0325 \; Hz \tag{4.8}$$

hence, considering that the vessel is moving away from the transmitter, the frequency becomes

$$f_1 \approx 324999.9675 \; Hz \tag{4.9}$$

We can now evaluate the magnitude response of the filter at the frequency f_1, which simulates the Doppler effect, and the frequency $f_2 = 324800$ Hz, which is the closest frequency of the MSK (neglecting the Doppler on the MSK). The objective is to maximize the magnitude at f_2 and minimize the magnitude at f_1. Minimizing the magnitude $|H(f_1)|$ is equivalent to maximize $1 - |H(f_1)|$. The Figure 4.7 illustrates the magnitude response of the notch filter at the two frequencies f_1 (solid blue line) and f_2 (dashed red line) function of the contraction factor. It ca be observed that an optimal point exists for

$$k_\alpha = 0.999913 \tag{4.10}$$

and with such constriction factor the 99.7% of the reference will be filtered, while the 99.7% of the the signal at f_2 will pass through the filter. The design

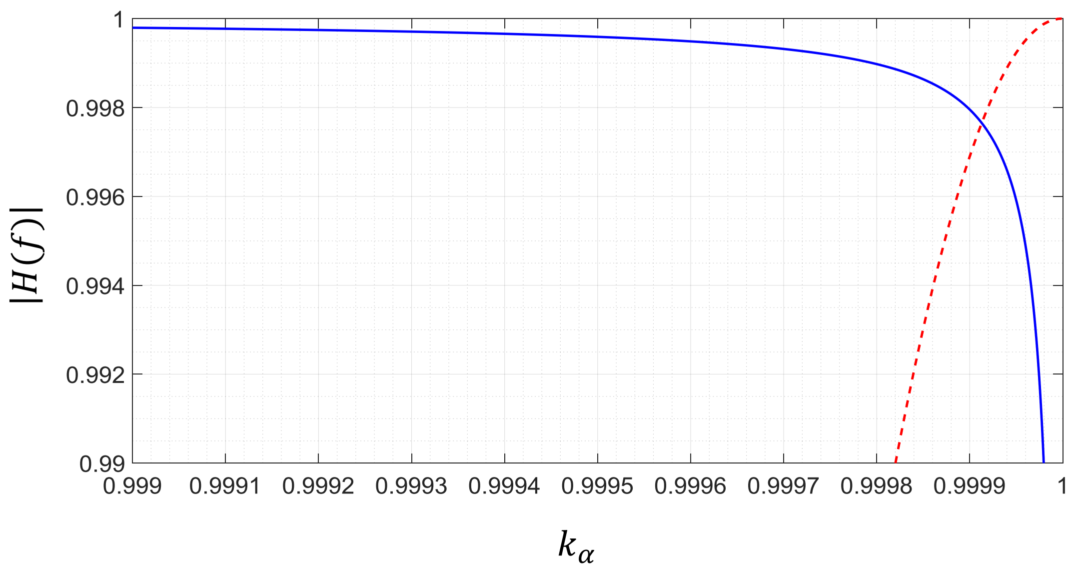

FIGURE 4.7: Magnitude response in linear scale at frequency f_1 ($1 - |H(f_1)|$) in blue and f_2 in dashed red

followed previously is not optimal but gives an approximated procedure to fix the contraction factor easily. Moreover, adaptive versions of the notch filter exist in the literature ([18] and [19]) which can be applied in order to follow and automatically adjust the target frequency in case of dynamic scenario.

The last point which is important to consider, is related to the stability of the filter. To guarantee the stability it is needed that the pole contraction factor has to be placed inside the unitary circle of the z-plane. Such conditions is satisfied for all the value of $k_\alpha < 1$, that, as said previously, is already satisfied.

Chapter 5

Phase Tracking Results

In Chapter 4 it is shown that a self-interference mitigation is needed to increase the accuracy of the estimated phase, therefore two techniques have been investigated in Section 4.1 and 4.2. In this chapter the results obtained for simulations and real recorded data are presented and analyzed; afterwards, a comparison of the performance is carried on.

For what concerns the simulations, the channel is assumed to be in three different noise conditions:

1. Noisless case
2. Medium noise case (AWGN with $C/N_0 = 45$ dB-Hz)
3. Severe noise case (AWGN with $C/N_0 = 30$ db-Hz)

Moreover, the simulated R-Mode signal is generated by using the following characteristics:

- Center frequency of the transmitter 300 kHz
- Starting phase of the signal $\theta = \pi$ rad
- Amplitude of the CWs $A_{CW} = 1$ and for the MSK $A_{MSK} = 4$

The following metrics are considered to evaluate the performance:

- Phase standard deviation (σ_θ)
- Phase maximum value ($\max(\theta)$), phase minimum value ($\min(\theta)$) and peak-to-peak variation ($\Delta\theta$)
- Phase mean value (μ_θ)
- Bias b respect to the true value

The total duration of the simulation is 80 s and the performances are evaluated between 60 s and 80 s, such that the transient is almost expired, whereas for the real measurement the last of two minutes phase tracking is taken into account. In all the cases, three processing approaches are applied:

- PLL-only: PLL without interference mitigation
- PLL-based: PLL with mitigation scheme as described in Section 4.1
- Notch-based: PLL with notch filter as described in Section 4.2

5.1 Simulated Static Scenario

In the static scenario, it is assumed that the receiver is in a fixed position, hence the Doppler is not present. The results presented in this section refer to the lower CW of the R-Mode signal which has a frequency of 299775 Hz.

5.1.1 Noiseless Channel

In the ideal channel condition we assume that there is no noise impacting on our signal. The PLL parameters are:

- $\zeta = 1/\sqrt{2}$
- $B_n = 0.5$ Hz

For the PLL-based mitigation the equivalent noise bandwidth for tracking the MSK is set to 3500 Hz as stated in section 4.1, while for the Notch-based mitigation it is important to remind that the constriction factor is set to 0.999913, as shown in section 4.2.

Figure 5.1 shows the estimated phase of the three different approaches. The plot at the top depicts the PLL-only approach, the middle plot represents the result with the Notch-based mitigation technique whereas the last plot is the one obtained with the PLL-based approach. In all the plots the blue line represents the estimated phase while the red dashed line indicates the reference value which is π rad. It is clear that, by using the PLL-only approach, the effect of the self-interference generated by the MSK brings to longer transient and higher standard deviation of the phase estimate. The notch based approach seems to be extremely effective against the interference. We can see that the transient is in line with the theoretical value ($\sim$ 7 s) and the accuracy of the phase estimation is greatly increased. The last approach, given by usage of the multi stage PLL, demonstrates that it is significantly effective against the interference in fact from 60 to 80 seconds the estimation is improved, but, on the contrary with respect to the Notch-based technique, it can be seen that the transient elongation is still present. On the other hand the PLL approach has one advantage, in fact it allows to track the MSK signal that can be used by the receiver to gather the bit information transmitted over the channel. Figure 5.2 depicts the results of the MSK phase tracking for a small amount of time. Reminding that the MSK bitrate is 100 bit/s, we can identify the bit information by evaluating the rate of change of the phase. If the phase increases the bit info is 1 whereas if it decreases the received bit is 0. As example, in Figure 5.2 the sequence of bits is given for the first 0.05 s.

However, the Figure 5.1 gives a visual perspective only, therefore two tables containing the numerical values of the performance metric are given. Table 5.1 contains the metric parameters in radians. It can be seen that the mitigation techniques reduce the standard deviation of the phase estimation and the peak-to-peak variation. Since the interest is to obtain ranges for positioning purpose, a better representation can be done by expressing the same parameters in meters. The Table 5.2 contains this information and the difference between the application of the PLL-only and the other two method which provide an interference mitigation is clear. The standard deviation drops from 4.7m to few centimeters and the peak to peak variation goes from 20 m to 26cm. The bias is also decreased from centimeter to millimeter level. These values demonstrate the the two developed techniques are able to provide good performance level. Of course this is valid under the assumption of zero noise on the channel, condition that is absolutely ideal therefore the performance with AWGN are assessed in the next sections.

Method	σ_θ	μ_θ	$\max(\theta)$	$\min(\theta)$	b	Δ_θ
PLL-only	0.0293	3.1429	3.2102	3.0789	-0.0014	0.1313
PLL-based	0.0001	3.1416	3.1421	3.1414	-0.0001	0.0007
Notch	0.0002	3.1416	3.1424	3.1407	-0.0001	0.0017

TABLE 5.1: Results for the static channel condition without noise in radians

Method	σ_θ	μ_θ	$\max(\theta)$	$\min(\theta)$	b	Δ_θ
PLL-only	4.679	500.240	510.958	490.954	-0.211	20.004
PLL-based	0.017	500.033	500.121	499.999	-0.002	0.122
Notch	0.039	500.031	500.161	499.902	-0.002	0.259

TABLE 5.2: Results for the static channel condition without noise in meters

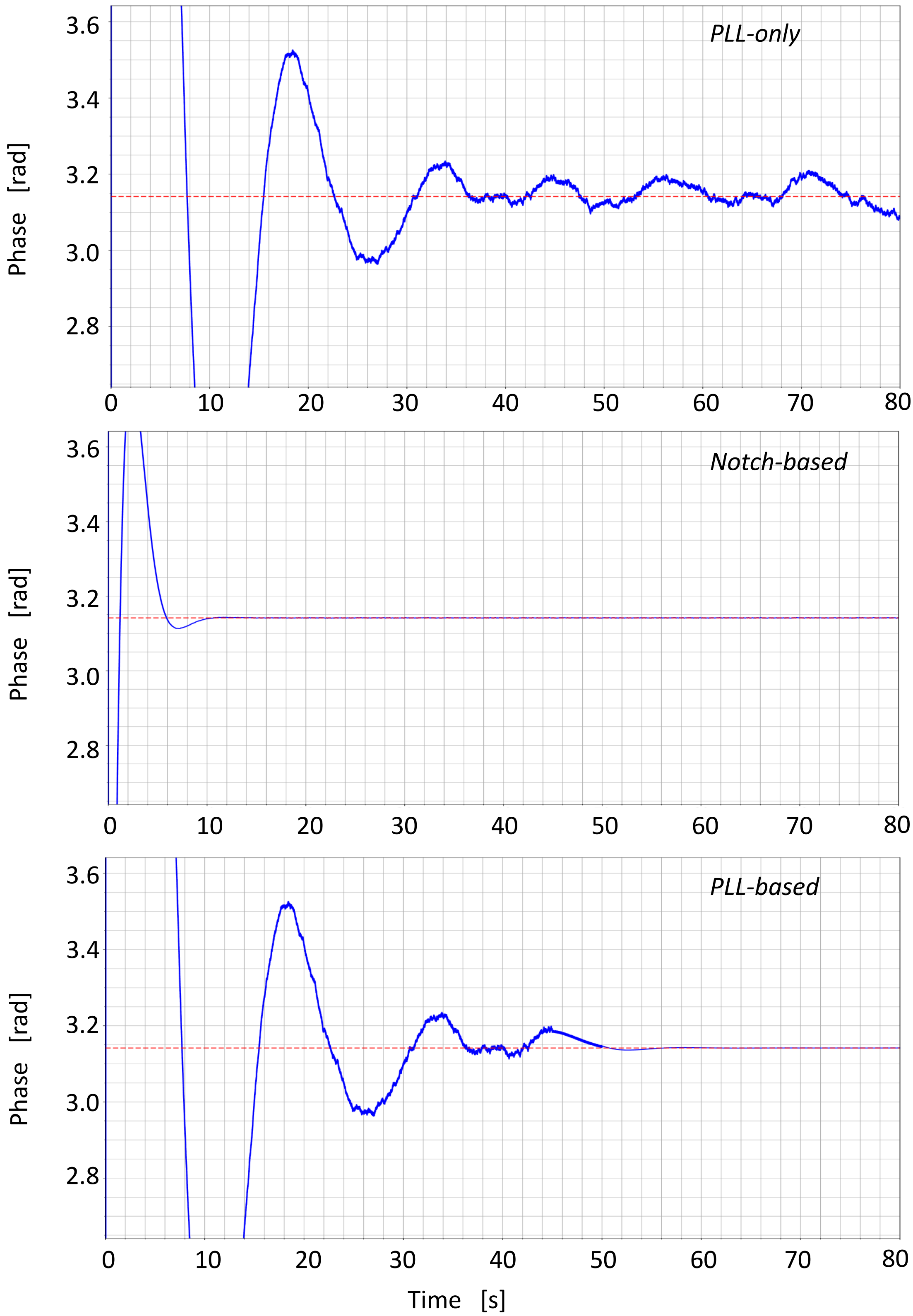

FIGURE 5.1: Phase estimation of the three approaches(PLL-only at the top, Notch-based mitigation at the middle and PLL-based mitigation at the bottom). In all the plots the blue continuous line represents the estimated phase while the red dashed line is the reference value.

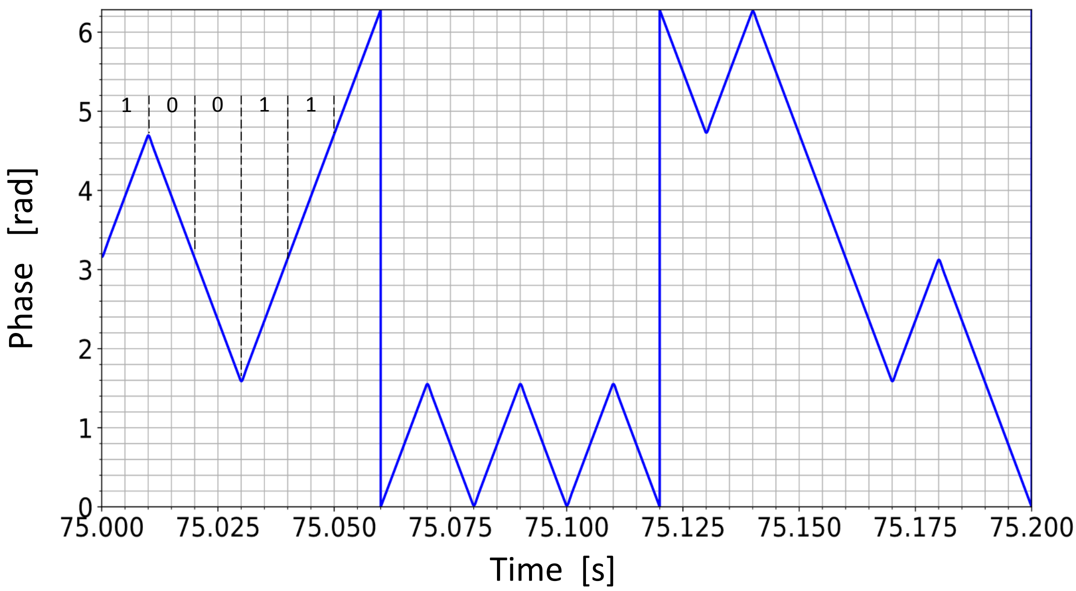

FIGURE 5.2: Phase estimation of the MSK signal. For the first 0.05s the bit information is given

5.1.2 AWGN with C/N_0 = 45 dB-Hz

In order to start considering a scenario which can be similar to a real one, the channel can be injected with additive white Gaussian noise (AWGN), and in this particular case the signal-to-noise density ratio (C/N_0) is set to 45 dB-Hz. The parameters for the PLL and the constriction factor of the notch filter are the same assumed previously.

Figure 5.3 depicts the results for this noisy case. The style is the same as in Figure 5.1, therefore the blue line is the phase estimate while the red dashed line is the reference value. As expected, by comparing Figures 5.1 and 5.3 it can be observed that in the second case (the noisy one) the estimation is not as good as in the first. If the time interval between 60 and 80 s is considered, the Notch-based and PLL-based performance decreases, as reasonably expected.

It is important to analyze the performance parameters, which are reported in the Table 5.3 and Table 5.4. To summarize the results, it can be noted that for

Method	σ_θ	μ_θ	$\max(\theta)$	$\min(\theta)$	b	Δ_θ
PLL-only	0.0290	3.1455	3.2168	3.0774	-0.0040	0.1394
PLL-based	0.0057	3.1418	3.1554	3.1285	-0.0003	0.0269
Notch	0.0055	3.1405	3.1550	3.1292	0.0010	0.0258

TABLE 5.3: Results for the static channel condition in radians with $C/N_0 = 45$ dB-Hz

Method	σ_θ	μ_θ	$\max(\theta)$	$\min(\theta)$	b	Δ_θ
PLL-only	4.767	500.664	512.013	489.821	-0.6357	22.192
PLL-based	0.920	500.071	502.237	497.958	-0.042	4.279
Notch	0.891	499.869	502.178	498.059	0.160	4.118

TABLE 5.4: Results for the static channel condition in meters with $C/N_0 = 45$ dB-Hz

all the three approaches the standard deviation, the bias and the peak-to-peak variation increase due to the presence of noise. However, also in this case, the mitigation techniques provide better performances with respect to the simple usage of the PLL alone. The PLL-based and the Notch-based approaches provides similar performance except for the bias which is slightly higher for the Notch approach. However, neglecting the small bias, they both can guarantee an accuracy of 1 meter (1 sigma) on the range.

Equation (3.23) is used to obtain the theoretical value of the standard deviation of the phase in case of AWGN and with this level of signal-to-noise ratio, the result is roughly 0.6 m. Such value is comparable with the standard deviation obtained with the mitigation techniques for which appears to be slightly higher.

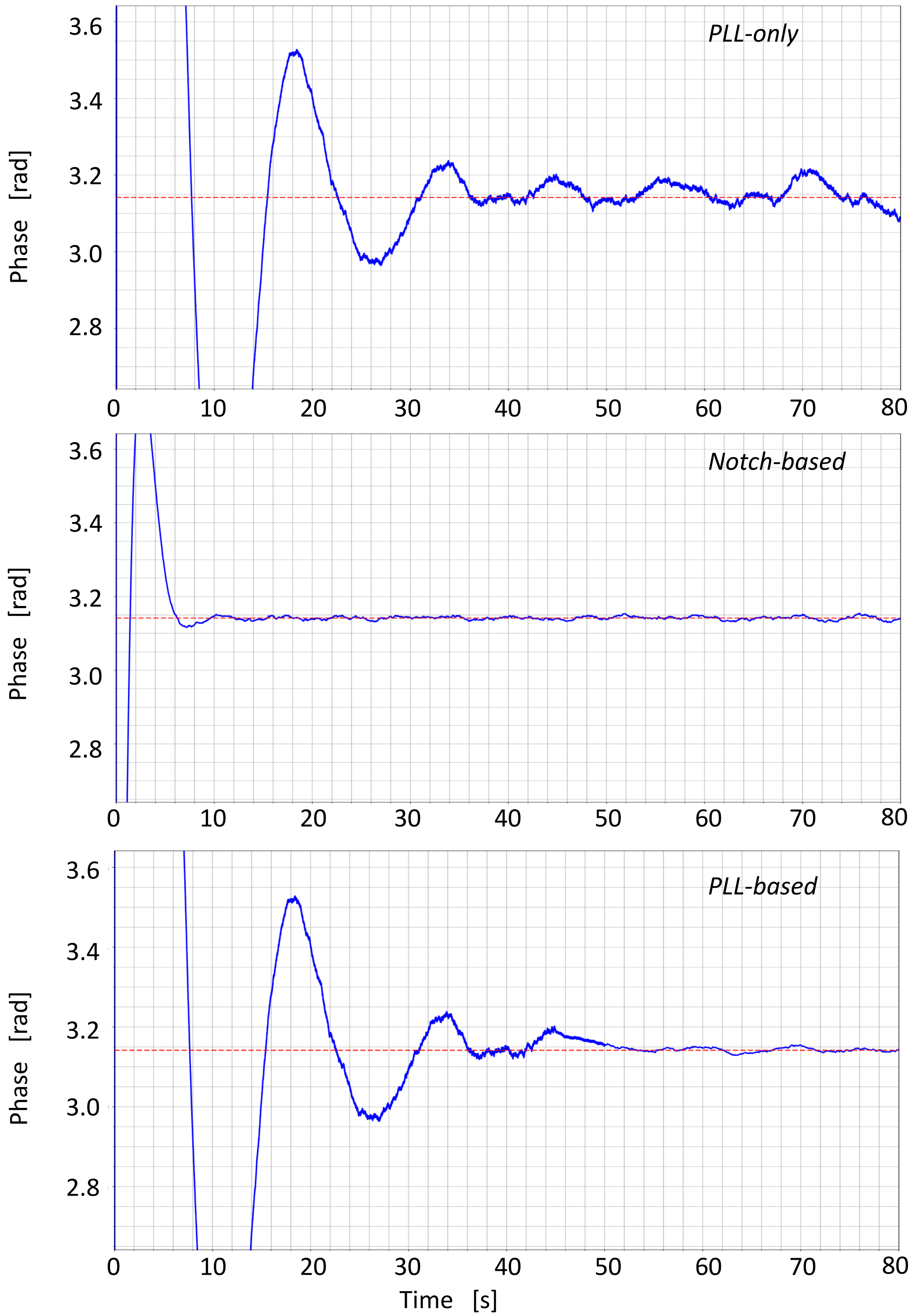

FIGURE 5.3: Phase estimation of the three approaches (PLL-only at the top, Notch-based mitigation at the middle and PLL-based mitigation at the bottom) with $C/N_0 = 45$ dB-Hz. In all the plots the blue continuous line represents the estimated phase while the red dashed line is the reference value π.

5.1.3 AWGN with C/N_0 = 30 dB-Hz

Similarly to the previous subsection, the simulation is repeated with a signal-to-noise density ratio of 30 dB, which is considered for the design of the PLL noise equivalent bandwidth, as in Section 3.2.

As for the previous cases, the Figure 5.4 represents the estimation of the phase. By looking at the picture, the difference with respect to the previous scenarios is clear. The estimation is significantly degraded, even for the two mitigation techniques. By reading the values in Table 5.5 and Table 5.6, it can

Method	σ_θ	μ_θ	$\max(\theta)$	$\min(\theta)$	b	Δ_θ
PLL-only	0,0211	3,1336	3,1953	3,0845	0,0079	0,1108
PLL-based	0,0235	3,1369	3,1884	3,0734	0,0046	0,1150
Notch	0,0208	3,1435	3,1899	3,0894	-0,0020	0,1005

TABLE 5.5: Results for the static channel condition in radians with $C/N_0 = 30$ dB-Hz

Method	σ_θ	μ_θ	$\max(\theta)$	$\min(\theta)$	b	Δ_θ
PLL-only	3,360	498,764	508,581	490,954	1,264	17,627
PLL-based	3,747	499,296	507,485	489,177	0,732	18,307
Notch	3,323	500,348	507,729	491,734	-0,319	15,995

TABLE 5.6: Results for the static channel condition in meters with $C/N_0 = 30$ dB-Hz

be noted that the standard deviation and the peak-to-peak variation become comparable among the three methods. Indeed, the noise at this point starts to become more significant than the effect of the interference itself causing the equalization of the performance levels.

The notch filter approach provides slightly better performance than the others. However, with the three approaches the standard deviation is in the order of 3.5 m which means an accuracy of 3.5 m (1 sigma) on the range estimation. By using (3.23) we can obtain the theoretical value of the standard deviation which is 3.5 m. This result is consistent to the values given in Table 5.6.

During the design procedure, the Doppler effect, due to the movement of the receiver, was considered, therefore the next section is dedicated to the performance in such condition.

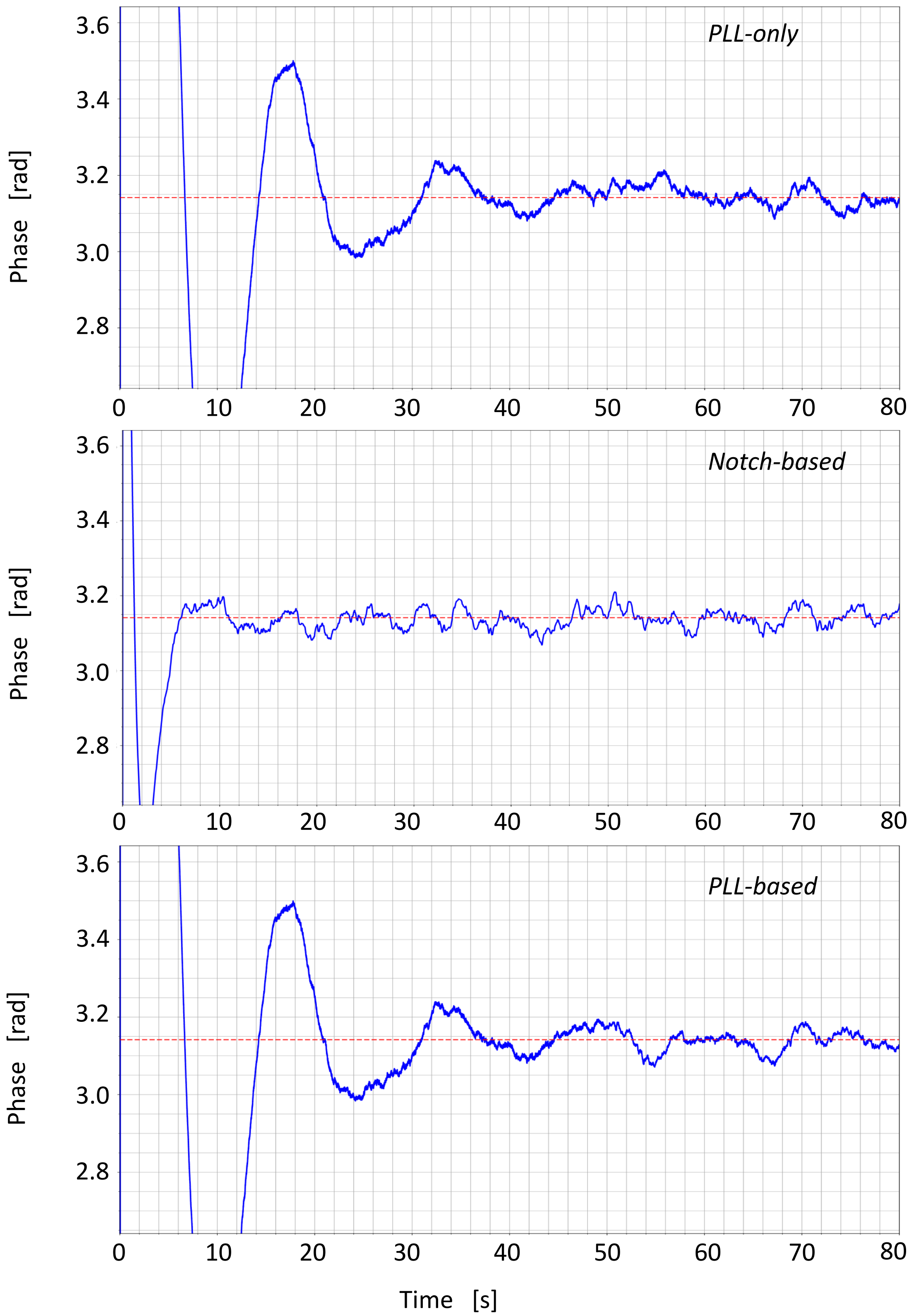

FIGURE 5.4: Phase estimation of the three approaches (PLL-only at the top, Notch-based mitigation at the middle and PLL-based mitigation at the bottom) with $C/N_0 = 30$ dB-Hz. In all the plots the blue continuous line represents the estimated phase while the red dashed line is the reference value π.

5.2 Simulated Dynamic Scenario

In the dynamic scenario the movement of the vessel, with respect to the transmitter, is simulated. Assuming that the vessel is moving toward the transmitter with a constant speed of 30 m/s, the frequency seen by the receiver is higher respect to the reference. The center frequency of the transmitter is 300kHz and, as for the static scenario, three different level of noise are taken into account (ideal, medium, high). Figure 5.5 represents the plot of the phase

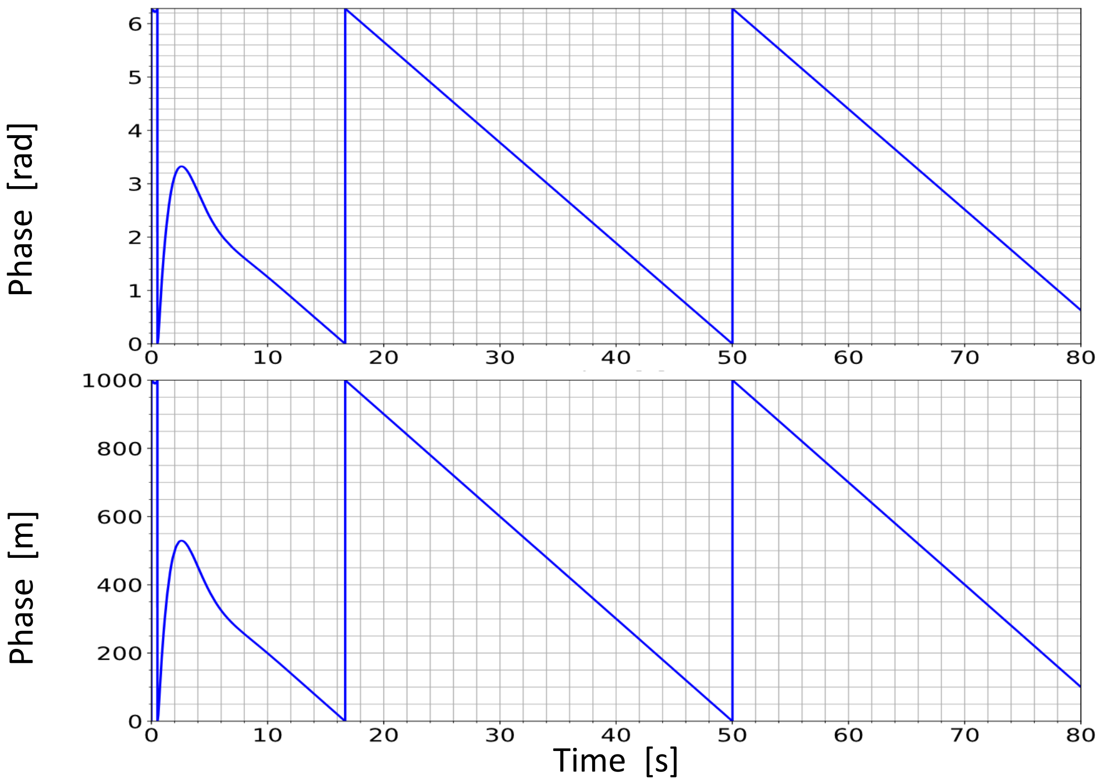

FIGURE 5.5: Phase estimation of notch filter approach without noise. The top plot is in radians whereas the bottom one in meters

for the notch approach without noise (at the top in radians and at the bottom in meters), and it can be observed that the phase difference, respect to the reference, is continuously varying in time and it is not constant anymore.This is perfectly expected, indeed this variation describes exactly the movement of the vessel. In the top plot, it can be noted that the phase values are in the range $0 - 2\pi$ as described in 2.1 and, once the ambiguity is fixed, with the PLL we can count the number of cycles to keep track of the range variation obtaining the full ranges at the chosen instant. Let's make a example: it is known that the phase value at time $t_0 = 0$ s is π which is equivalent to 500 m. Each cycle at this frequency is roughly equivalent to 1 km; by supposing that the vessel at time zero is 10.5 km far from the transmitter, the ambiguity N is equal to 10 which is equivalent to 10 km. In the plot in meters it can be seen that at time $t_0 = 0$ s the PLL is in the transient hence the observation at that time is not valid. At time $t_1 = 10$s, the phase is 200 m and, since the cycle is the same, the ambiguity N is still 10. Therefore, the full range after 10 seconds is 10.2 km. Observing that the difference between the full range at time t_0 and t_1 is 300 m, it can be concluded that this is equivalent to the vessel movement in 10 seconds by maintaining a constant speed of 30 m/s toward the transmitter. In a similar way, at time $t_2 = 20$ s the observation gives 900 m, but the ambiguity now is decreased by 1 hence the full range is 9.9 km.

The plots for the other approaches are omitted, to avoid redundancy, and only the tables with the performance metric are presented. In order to evaluate the metric, the CW with Doppler frequency is used as reference signal. The phase mean value is omitted due to the fact that it continuously vary as shown in Figure 5.5. The standard deviation(σ_θ) maximum and minimum deviation (max($\Delta\theta$), min($\Delta\theta$)) from the reference and the peak-to-peak variation (Δ_θ) and the bias (b)are given in the following tables.

Noiseless [rad]					
Method	σ_θ	max($\Delta\theta$)	min($\Delta\theta$)	b	Δ_θ
PLL-only	0.0118	0.0408	-0.0294	-0.0165	0.0702
PLL-based	0,0001	0.0002	-0.0001	-0.0001	0,0003
Notch	0,0004	-0.0008	-0.0035	-0.0021	0,0027

Noiseless [m]					
Method	σ_θ	max($\Delta\theta$)	min($\Delta\theta$)	b	Δ_θ
PLL-only	1,880	6.482	-4.681	-2.611	11,163
PLL-based	0,013	0.045	-0.013	-0.004	0,058
Notch	0,073	-0.114	-0.553	-0.335	0,439

TABLE 5.7: Results for the dynamic channel condition without noise (at the top results in radians while at the bottom in meters)

By comparing the tables obtained in section 5.1 withe Table 5.7, 5.8 and 5.9, it is clear that the same trend in terms of performance is obtained. The mitigation techniques improve the performance of the estimation in all the three cases of C/N_0. Although most of the dynamic scenario performance parameters are similar to the static ones, for some of them it appears that they are slightly different. However, these results are related to one particular realization and it is clear that a more formal approach would be to perform a Monte Carlo simulation by varying the diverse variables that could impact on the PLL in order to increase the statistical meaning of the results. Nevertheless, such work of test and simulation would require extremely high effort from the processing time and hardware resources point of view. Indeed each simulation last approximately 4 h and by considering only one set of starting phase for

$C/N_0 = 45$ dB-Hz [rad]					
Method	σ_θ	$\max(\Delta\theta)$	$\min(\Delta\theta)$	b	Δ_θ
PLL-only	0,0138	0.0476	-0.0280	-0.0181	0,0756
PLL-based	0,0046	0.0152	-0.0090	-0.0027	0,0242
Notch	0,0033	0.0073	-0.0119	0.0014	0,0192

$C/N_0 = 45$ dB-Hz [m]					
Method	σ_θ	$\max(\Delta\theta)$	$\min(\Delta\theta)$	b	Δ_θ
PLL-only	2,208	7.582	-4.447	-2.874	12,029
PLL-based	0,745	2.429	-1.431	-0.422	3,860
Notch	0,534	1.171	-1.891	0.023	3,062

TABLE 5.8: Results for the dynamic channel condition with $C/N_0 = 45$ dB-Hz (at the top results in radians while at the bottom in meters)

the CW and an MSK with the same bit sequence repeated 1000 times means roughly 5 months of processing, which is not feasible.

Nevertheless, it is important here to underline the fact that in case of dynamic conditions the receiver can still operate with the three approaches without dramatic loss of performance. Also in this case the Notch filter approach seems to be the best choice indeed it provides the smallest standard deviation on the phase estimate in a noisy channel with respect to the others, moreover its convergence time is not increased and this means that the receiver can obtain the observation earlier or eventually the bandwidth can be further decrease in order to improve the performance as will be shown for the real measurement case.

$C/N_0 = 30$ dB-Hz [rad]					
Method	σ_θ	$\max(\Delta\theta)$	$\min(\Delta\theta)$	b	Δ_θ
PLL-only	0.0425	0.1193	-0.0586	-0.0150	0.1779
PLL-based	0.0223	0.0500	-0.0575	0.0054	0.1075
Notch	0.0193	0.0492	-0.0308	-0.0096	0.0800

$C/N_0 = 30$ dB-Hz [rad]					
Method	σ_θ	$\max(\Delta\theta)$	$\min(\Delta\theta)$	b	Δ_θ
PLL-only	6.780	19.002	-9.614	-2.377	28.617
PLL-based	3.553	7.969	-9.146	-0.725	17.115
Notch	3.072	7.845	-4.886	-1.517	12.732

TABLE 5.9: Results for the dynamic channel condition with $C/N_0 = 30$ dB-Hz (at the top results in radians while at the bottom in meters)

5.3 Real Measurement Results

The DLR is implementing the R-Mode receiver using an SDR and its block diagram is depicted in Figure 5.6. The Ettus N210 with LFRX daughterboard is used as SDR which is time synchronized with a LL-3760 Lange Electronic GNSS stabilized rubidium clock. The receiver is synchronized to the Universal Coordinated Time (UTC) through a pulse per second (PPS) signal. On the second output the clock provides a 10 MHz sine-wave signal which allows for stable measurements [20]. On the MF front end a H-field loop antenna with two amplification stages is used and then the signal is recorded on a PC and analyzed in post-processing. The signal considered for the real case was

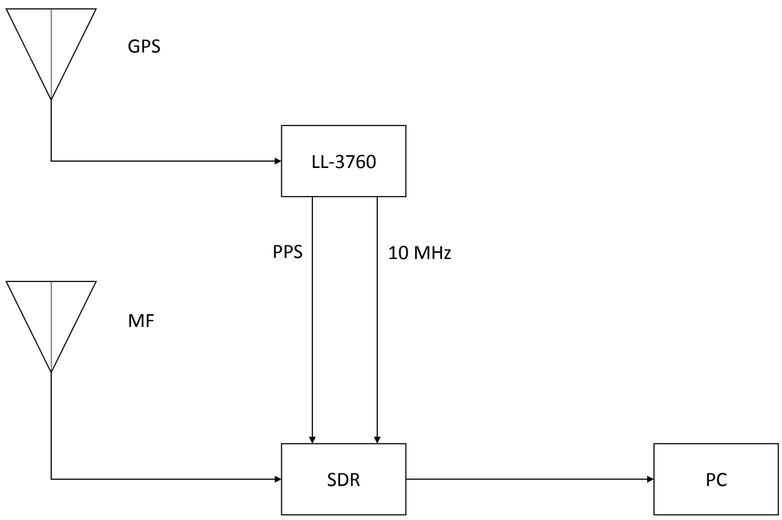

FIGURE 5.6: R-Mode receiver block diagram [20]

recorded in Dorum (Germany) during a measurement campaign conducted in July 2019. The sampling frequency of the signal is 1 MHz and the spectrum of the R-Mode signal coming from Zeven (Germany) is depicted in Figure 5.7. By observing the figure it is easy to see the two continuous waves represented by the two spikes and the main lobe of the MSK centered among them; furthermore we can roughly evaluate the C/N_0 level which is 43 and 39 dB-Hz for the low CW and the high CW respectively. From the spectrum it can be checked that the central frequency of the station situated in Zeven is 303.5 kHz and the continuous waves are located at 303.225 and 303.725 kHz.

As for the simulation, the three processing PLL approaches are applied by using the usual parameters described previously, and the performance are

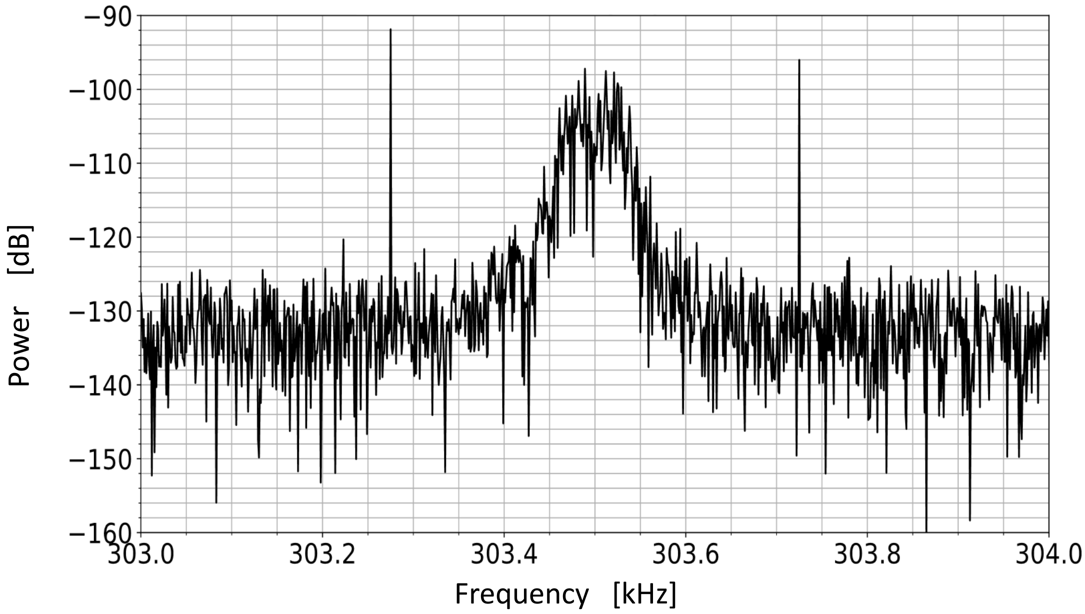

FIGURE 5.7: Power density spectrum of the Zeven R-Mode signal captured in Dorum (July 2019)

summarized in Tables 5.10 and 5.11. These values, used for performance evaluation and described at the beginning of this chapter, are obtained by considering only the last 60 seconds of 2 minutes phase tracking, as shown in Figure 5.8. Clearly, the bias b has not been examined since there is not a reference value for the phase.

By reading the Tables 5.10 and 5.11, it easily appears that the PLL-only has lower performance respect to the PLL-based and Notch-based approaches, as expected from the simulation results. Furthermore, by comparing the results in Table 5.10 with the ones in Table 5.11, it can be noted that different level of performance are obtained for the two CW. In particular, the values of standard deviation and peak-to-peak variation for the high CW are higher than the low CW ones, which means that the accuracy is lower for the first case. This outcome can be easily explained by the fact that the two CW are characterized by different C/N_0 levels and, as shown in the theory and simulation sections, to smaller values of carrier-to-noise density ratio correspond lower performance.

As expected from the simulation results described in Sections 5.1 and 5.2, it can be also noted that the notch filter combined with the PLL is characterized by the best performance (in terms of standard deviation and peak-to-peak variation), moreover it is important to remind that such approach is not affected by an increase of transient time (which means that it converges faster to the steady state value) and the complexity of such implementation is minimal. One more advantage of the Notch-based technique compared to the PLL-based technique is that it does not depend on the tracking of the other CW which implies higher reliability. In fact, if one CW tracking is lost the other is not affected and a range estimation is still possible. For these aforementioned reasons, the suggested processing technique chosen for the R-Mode phase tracking is the PLL with Notch-based approach described in Section 4.2.

Low CW [rad]					
METHOD	σ_θ	μ_θ	$max(\theta)$	$min(\theta)$	Δ_θ
PLL-only	0.0159	6.02596	6.0719	5.9777	0.0942
PLL-based	0.0081	5.9725	5.9959	5.9505	0,0454
Notch	0.0074	5.9909	6.0127	5.9686	0.0441
Low CW [m]					
METHOD	σ_θ	μ_θ	$max(\theta)$	$min(\theta)$	Δ_θ
PLL-only	2.507	948.042	955.276	940.469	14.806
PLL-based	1.287	939.646	943.332	936.190	7.141
Notch	1.167	942.547	945.962	939.035	6.926

TABLE 5.10: Results for low CW recorded signal (at the top results in radians while at the bottom in meters)

High CW [m]					
METHOD	σ_θ	μ_θ	$max(\theta)$	$min(\theta)$	Δ_θ
PLL-only	0.0376	5.0086	5.1088	4.9155	0.1933
PLL-based	0.0154	5.0574	5.0969	5.0183	0,0.0786
Notch	0.0125	5.0235	5.0571	4.9879	0.0692
High CW [m]					
METHOD	σ_θ	μ_θ	$max(\theta)$	$min(\theta)$	Δ_θ
PLL-only	5.923	787.980	803.763	773.357	30.406
PLL-based	2.431	795.680	801.891	789.528	12.363
Notch	1.982	790.337	795.635	784.739	10.896

TABLE 5.11: Results for high CW recorded signal (at the top results in radians while at the bottom in meters)

During the design process described in Section 3.2, seven seconds of locking time were considered in order to acquire quickly the phase of the CW. This choice was taken due to the fact that the PLL-only and PLL-based mitigation techniques are affected by longer convergence time. Therefore, by only considering the notch filter approach, this constraint can be relaxed and the equivalent noise bandwidth of the PLL can be slightly decreased. For instance, with a noise equivalent bandwidth of 0.08 Hz a transient of roughly 43 s is calculated by using (2.57). This reduction in the loop bandwidth implies a huge enhancement in the performance level, as can be seen in Tables 5.12 and 5.13 which refer to low and high CW respectively. In fact, the standard deviation decrease from 1.16 m to 0.32 m for the low CW and from 1.98 m to 1.08 m for the high CW. Also the peak-to-peak variation is reduced to 1.75 m and 4.63 m for the low and high CW respectively. This means that the accuracy of the phase measure is approximately 1 m (3 sigma) for the low CW and 3.24 m (3 sigma) for the high CW.

Nevertheless, this is not the accuracy on the final position estimation but assuming a HDOP of 2, as reported in Section 1.3, and considering the 3 sigma standard deviation of the low CW, the final accuracy on the position can be better than 2 m for the 98.9 % of the time, condition that satisfy the safe requirements for navigation suggested by the IMO. In the case the high Cw standard deviation is considered, an accuracy of 6.48 m is obtained, which is still below the 10 m limit.

In order to validate the results, the DTFT technique, as described in Section 2.2.1, is applied by using one million samples and since the sample rate is 1MS/s one estimation per second is produced. The performance of the DTFT approach is reported in Tables 5.12 and 5.13. It can be noted that the Notch approach and the DTFT provide similar results, however the PLL combined with the notch filter performs better than the DTFT with 1 MS. Indeed the improvement of performance for the Notch-based approach is roughly 1 m on the standard deviation and 4 m on the peak-to-peak variation for both the CW. These results are represented in Figure 5.9 which shows the comparison between the DTFT and the PLL with the Notch filter, furthermore the scale of the pictures is equal to the scale proposed in Figure 5.8 in order to visually compare them.

Low CW [rad]					
METHOD	σ_θ	μ_θ	$max(\theta)$	$min(\theta)$	Δ_θ
Notch	0.0020	5.9911	5.9969	5.9858	0.0111
DTFT	0.0075	5.9907	6.0100	5.9705	0.0395
Low CW [m]					
METHOD	σ_θ	μ_θ	$max(\theta)$	$min(\theta)$	Δ_θ
Notch	0.329	942.577	943.487	941.732	1.754
DTFT	1.187	942.501	945.537	939.337	6.200

TABLE 5.12: Performance comparison between DTFT and Notch-based PLL for low CW recorded signal (at the top results in radians while at the bottom in meters)

Evidently, the reduction of the noise equivalent bandwidth for the PLL brings to performance improvement in the accuracy of the phase estimation,

High CW [m]					
METHOD	σ_θ	μ_θ	$max(\theta)$	$min(\theta)$	Δ_θ
Notch	0.0068	5.0243	5.0377	5.0082	0.0295
DTFT	0.0130	5.0238	5.0488	4.9922	0.0566

High CW [m]					
METHOD	σ_θ	μ_θ	$max(\theta)$	$min(\theta)$	Δ_θ
Notch	1.081	789.297	791.402	786.762	4.639
DTFT	2.047	789.217	793.153	784.249	8.904

TABLE 5.13: Performance comparison between DTFT and Notch-based PLL for high CW recorded signal (at the top results in radians while at the bottom in meters)

as already discussed in Section 3.2, but attention must be payed to the convergence time and to the capability of the PLL to follow the evolution of the signal in case of dynamic receiver.

As explained in section 2.2.1, the DTFT phase estimation can be also improved by increasing the number of samples. Although the increase of the observation time brings to higher accuracy, there is a main drawback: the information is averaged therefore the phase estimate in a dynamic scenario can be corrupted. The DTFT is not able to follow the evolution of the signal sample by sample, in fact in order to increase its ability to adapt to a frequency change in a dynamic scenario a decrease of the observation time or the number of samples is needed. It is true that the expected Doppler is very limited but this effect brings anyway to a larger error compared to the PLL.

On the other hand, the PLL is inherently able to adapt sample by sample to signal dynamic variation as discussed in Section 3.2.

These are the main advantages which motivate the use of PLL in place of DTFT technique that is, at the time of writing, used for the MF R-Mode phase estimate. Nevertheless there is a drawback, indeed to each CW must be associated a PLL running in real-time, which causes a larger usage of resources respect to DTFT. For instance, in a SDR receiver a multi-thread approach is needed in order to run the PLL in parallel. Although nowadays this is not a great issue from the processing power point of view neither form an energy power consumption perspective. Indeed, the target users are vessel which typically do not suffer lack of electrical power. Differently, the DTFT can estimate the phase of all the CW in one shot, which is surely more efficient than the PLL in terms of resources exploitation.

It is fundamental to remind that the phase measured by the PLL, as showed in the Figure 5.8 and 5.9, does not provide the final range used in the position solver, indeed the measurement is affected by the ambiguity as explained in Section 2.1. This issue must be solved in order to obtain the ranges and the position but addressing such topic is out the scope of the thesis. However, one of the possible suggested solution considered is to use the beat frequency signal. Nonetheless, such solution requires high accuracy on the estimation of the phase (roughly tens of centimeters) which can be potentially achieved by reducing the equivalent noise bandwidth paying, on the other side, in terms of convergence time.

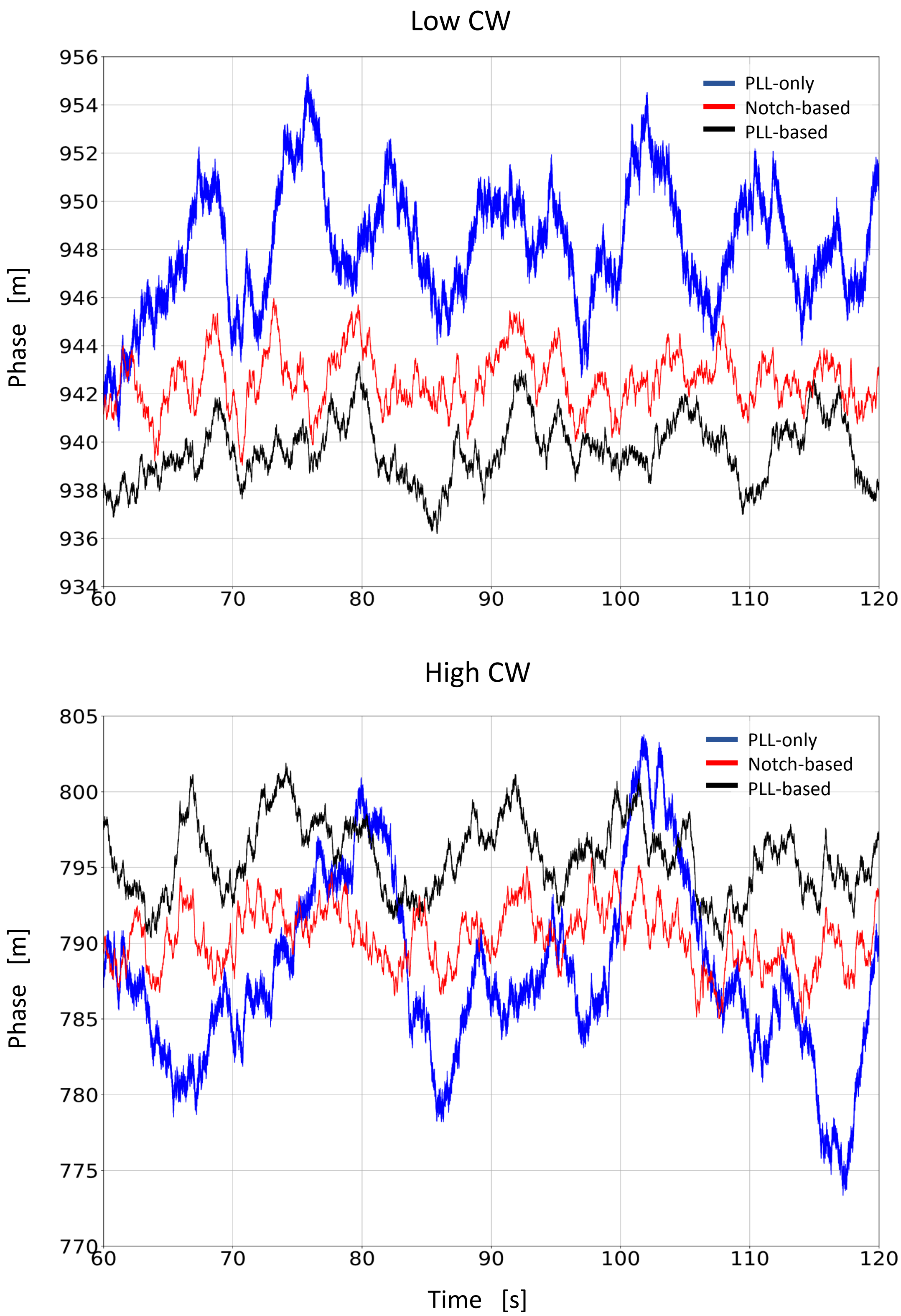

FIGURE 5.8: Zeven R-Mode signal phase tracking in meters of the low CW (top) and high CW (bottom) for 1 minute

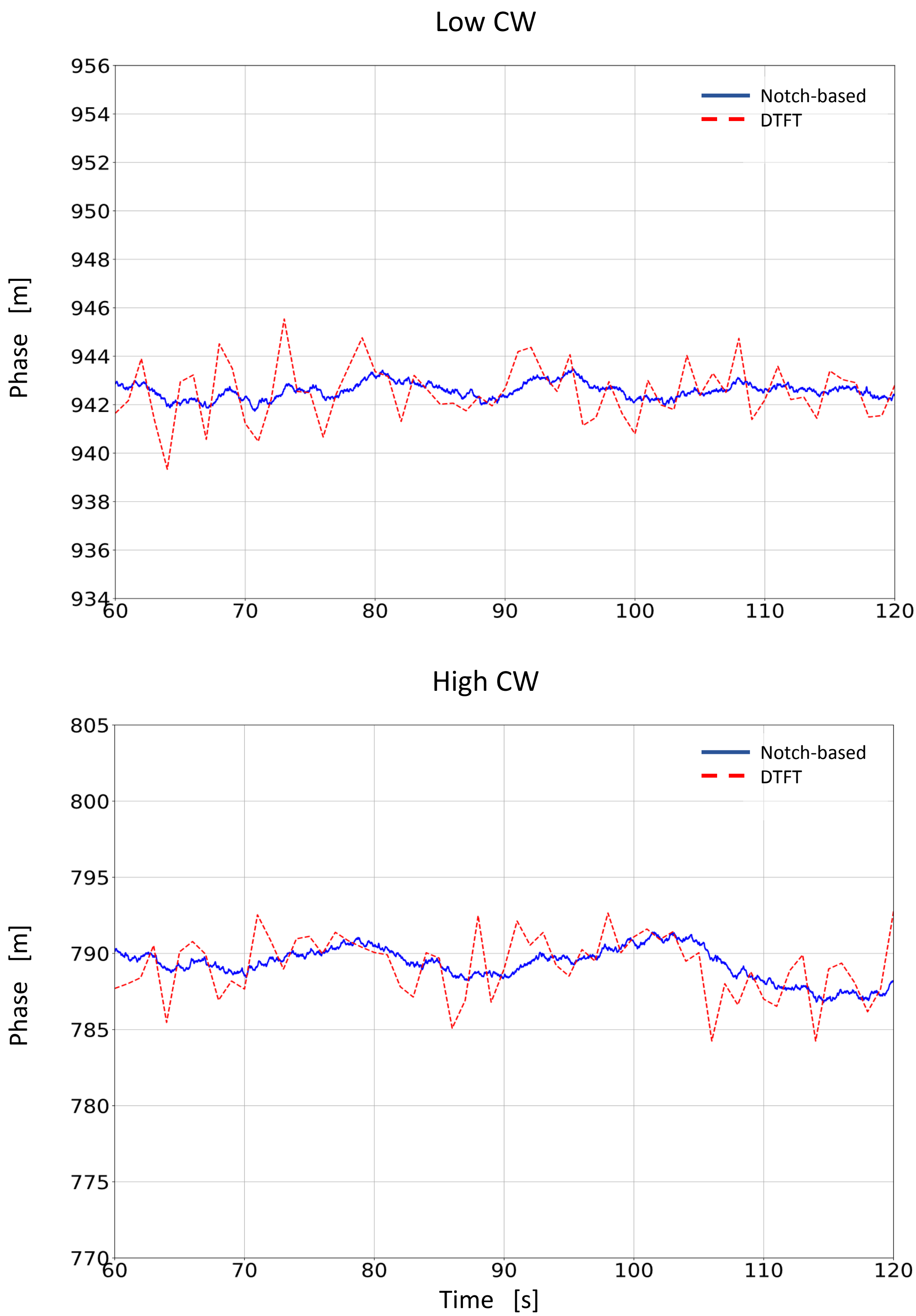

FIGURE 5.9: DTFT vs Notch-based PLL of Zeven R-Mode signal phase tracking in meters of the low CW (top) and high CW (bottom) for 1 minute

Chapter 6

Conclusion

This thesis presents a new approach, with respect to the DTFT and ML techniques, to provide stable phase measurements for the MF R-Mode signal which will be exploited to obtain range measurements and finally a position estimation of the vessels in the maritime domain. As explained in the introduction, the principles and a design approach for the fixed parameters R-Mode PLL are described. Sections 5.1, 5.2 and 5.3 demonstrate the potential benefits offered by the application of PLL with its high accuracy on the phase estimation and its capability to properly work in a dynamic scenario, which was tested only in simulation due to the lack of real recorded measurements in such condition. The simulation results illustrate that the PLL tracking of the CW is affected by a self-interference produced by the presence of the R-Mode MSK component which induces a loss of performance. Therefore, two mitigation schemes were proposed and analyzed resulting very effective against this interference. The applicability of the PLL combined with the mitigation approaches, the first based on multiple PLL_s running in parallel whereas the second based on the notch filter, with its performance level was proven not only in the simulated and controlled environment but also in the real measurement case. Among the proposed techniques, the notch filter followed by the PLL has shown the best performance in terms of accuracy and convergence time.

Though not claiming to be an exhaustive analysis of all the possible scenarios which may impact the accuracy of the measurements (e.g. skywave, noise level, in-band interference), it has been shown that the performance requirements proposed by the IMO resolutions can be satisfied with the combination of PLL and notch filter. As shown in Section 5.3 for the real measurement results, if an HDOP of 2 is considered as explained in Section 1.3, it can provide 2 m accuracy (3 sigma) with 98.9 % probability considering the low CW standard deviation. If the high CW standard deviation is considered, the accuracy decreases to 6.5 m (3 sigma) due to the lower C/N_0 level. These results were compared with the 1 MS DTFT technique which results to have a standard deviation four times larger for the low CW and two times for the high CW, therefore the PLL has shown to perform better.

Although, better performance are possibly achieved by PLL if the loop noise equivalent bandwidth is reduced, further investigation is needed to find the operational limits of the proposed processing technique, always considering the constraint on the convergence. However, it is important to underline the fact that few realizations of the signal are used for the simulation and one data set for the real measurement results, therefore a deeper analysis must be conducted on additional data collection in order to increase the statistical significance of the results. Moreover the ranges shown in Sections 5.1, 5.2 and 5.3 are not used to solve the navigation equation since they are affected by ambiguity, as explained in Section 2.1. Therefore, this issue must be addressed and one possible solution is to exploit the beat frequency signal of the CW_s [10].

In this work the PLL design considers fixed parameters which can not be changed on-line during the processing and it has been shown that the PLL performance strictly depends on such parameters, e.g. the loop noise equivalent bandwidth the damping factor and the constriction factor of the notch filter. Consequently, the adoption of adaptive version of PLL and notch filters, that already exists in the literature, may be fundamental in order to improve the receiver capability to work on different scenarios. In fact, the adaptive capacity of the receiver can potentially allow to satisfy a minimum performance requirement in a time variable environment making the navigation safer and more reliable. A future work could be devoted to investigate toward this direction which may significantly improve the system performance extensively encouraging the potential users to adopt the R-Mode receiver on board of vessels.

Bibliography

[1] P. Misra and P. Enge. *GLOBAL POSITIONING SYSTEM. Signals, Measurements, and Performance*. 2nd ed. Lincoln, Massachusetts 01773: Ganga-Jamuna Press, 2006.

[2] European Space Agency. *Navipedia*. 2018. URL: https://gssc.esa.int/navipedia/index.php/Main_Page.

[3] Dana Goward. *GPS disrupted for maritime in Mediterranean, Red Sea*. 2018. URL: https://www.gpsworld.com/gps-disrupted-for-maritime-in-mediterranean-red-sea/. (accessed: 23.01.2020).

[4] Emilio Marcos et al. "Interference awareness and characterization for GNSS maritime applications". In: *IEEE/ION Position, Location and Navigation Symposium (PLANS)* (Apr. 2018), pp. 908–919.

[5] Daniel Medina et al. "On GNSS Jamming Threat from the Maritime Navigation Perspective". In: *22th International Conference on Information Fusion (FUSION)* (July 2019), pp. 1–7.

[6] Lars Grundhöfer et al. "Characterization of a Transmitter in a Medium Frequency Maritime Terrestrial Navigation System". In: *IEEE Intelligent Transportation Systems Conference (ITSC)* (Oct. 2019), pp. 3828–3832.

[7] Johnson Gregory and Swaszek Peter. *Feasibility Study of R-Mode combining MF DGNSS, AIS, and eLoran Transmissions*. 2014.

[8] Jan Safar. *AIS/VDES R-Mode Development*. 2018.

[9] *R-Mode website*. 2019. URL: http://r-mode-baltic.eu/. (accessed: 23.01.2020).

[10] Gregory Johnson and Peter Swaszek. *Feasibility Study of R-Mode using MF DGPS Transmissions*. 2014.

[11] IMO Resolution A.953(23). *WORLD-WIDE RADIONAVIGATION SYSTEM*. 2014.

[12] David C. Rife and Robert R. Boorstyn. "Single-Tone Parameter Estimation from Discrete-Time Observation". In: *IEEE TRANSACTIONS ON INFORMATION THEORY* 5 (Aug. 1974), pp. 591–598.

[13] Michael Rice. *Digital Communications: A Discrete-Time Approach*. Upper Saddle River, New Jersey 07458: Prentice Hall, 2009.

[14] R.W. Stewart et al. *Software Defined Radio using MATLAB® Simulink® and the RTL-SDR*. 1st ed. Glasgow, Scotland, UK: Strathclyde Academic Media, 2017.

[15] Donald R. Stephens. *Phase-Locked Loops For Wireless Communications. Digital and Analog Implementation*. New York: Springer Science+Business Media, 1998.

[16] Roland E. Best. *Phase-Locked Loops. Design, Simulation, and Application*. 5th ed. McGRAW-HILL, 2003.

[17] Alan V. Oppenheim, Alan S. Willsky, and S. Hamid Nawab. *Signals & Systems*. Upper Saddle River, New Jersey 07458: Prentice Hall, 1996.

[18] Qin Wenjian et al. "A Comparison of Optimized Mitigation Techniques for Swept-frequency Jammers". In: *Proceedings of the 2019 International Technical Meeting of The Institute of Navigation* (Jan. 2019), pp. 233–247.

[19] Daniele Borio. "Loop analysis of adaptive notch filters". In: *IET Signal Processing* 10 (Feb. 2016), pp. 659–669.

[20] Lars Grundhöfer and Stefan Gewies. "R-Mode receiver development for medium frequency signals". In: *Scientific Journals of the Maritime Univeristy of Szczecin* (Dec. 2018), pp. 57–62.